(2)

AR-006-974



DSTO AUSTRALIA

ELECTRONICS RESEARCH LABORATORY



# Electronic Warfare Division

RESEARCH REPORT
ERL-0634-RR

## A TIME DOMAIN SIMULATION OF THE PULSED RADAR RETURN FROM A CHAFF CLOUD

Thomas A.Winchester

ABSTRACT

A numerical technique for the time domain simulation of the radar return from a chaff cloud is developed. This technique is suitable for pulsed radars. A Monte-Carlo analysis of the effect of this return upon the range discriminant of typical pulsed radar systems is then carried out.



May 1992 COPY No.



APPROVED FOR PUBLIC RELEASE

Postal Address: Director, Electronic Research Laboratory,
PO Box 1500, Salisbury, South Australia, 5108.

# CONTENTS



# FIGURES

## TABLES



## APPENDICES



## FIGURES



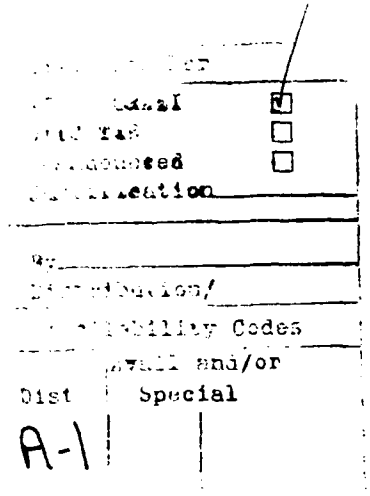

THIS IS INTENTIONALLY BLANK

# 1 INTRODUCTION

Chaff can be used for the protection of ships, by using it in the seduction mode or the confusion mode. In the seduction mode the inbound Anti-Ship Missile (ASM) transfers lock onto the chaff cloud in preference to the ship. One obvious requirement for the success of this technique is that the perceived radar cross section of the chaff cloud is large relative to that of the ship. However, a chaff cloud is an extended target, and the notion of radar cross section strictly applies only to point targets. If the missile seeker is to track the chaff cloud in preference to a ship target, then the effect of a chaff cloud upon the shape of the signal returned as processed by the individual radar system needs to be analysed. Since a chaff cloud consists of a large number of individual scatterers randomly distributed in space and orientation, the shape of the returned signal is a statistical quantity.

At recent trials held at the Proof and Experimental Establishment, Port Wakefield, the radar cross sections of some shipboard chaff rounds were measured using an instrumented Cyrano Radar. The author was present at these trials, and noted the appearance of the time domain return of the chaff cloud, as displayed on a A-scope. It consisted of a large number of peaks whose lifetime was of the order of one second, or less. Hence, the statistical nature of the return of the chaff cloud cannot be neglected in assessing the effect of this return upon the radar system. Since the range discriminant must be a non-linear transformation of the signal, we require a random sample of the returned signal so that we can perform a Monte-Carlo analysis of its effect upon the range discriminant.

In this report we develop a technique which simulates the time domain return from a large number of stationary scatterers. Since pulsed radars have poor doppler resolution, this technique is suitable for pulsed radars. We also assume that multiple incoherent scattering can be neglected (conditions for this are derived in Section 2), although many of our conclusions will be seen to be insensitive to this assumption. The key to this technique is that the effect of a cloud of stationary scatterers upon the returned signal can be manipulated as if it were the spectral representation of a strictly band limited stationary complex Gaussian random series in frequency space. By generating a random sample of this random series in frequency space, and using convolution integrals, a random sample of the return of this type of cloud can be generated. The numerical implementation of this scheme is easier if we treat the signal after it has been processed by a matched filter; that is, if we obtain a sample of the video signal. A Monte-Carlo analysis of the returned signal as processed by the detector is performed, and compared to the some analytical results. The range discriminant is then subjected to the same Monte-Carlo analysis. Various statistical characteristics of the range discriminant are then obtained, and related to features of the chaff cloud.

# 2 THEORY

## 2.1 First Order Multiple Scattering Theory

As an incident wave propagates through a cloud of scatterers, it loses energy due to scattering and absorption by the scatterers. Since chaff is intended to reflect strongly, the dominant process we shall be concerned with is scattering rather than absorption. The incident energy flux (or the power of the coherent wave) within the cloud due to a radar beam is given by (Ishimaru 1978):

$$S_i = P_t \frac{G_t(\hat{i})}{4\pi R^2} \exp(-\gamma) \qquad 2.1.1$$

$$\gamma = \int_0^R \rho \langle \sigma_t(\hat{i}) \rangle ds \qquad 2.1.2$$

Here, $S_i$ is the incident flux, $G_t(\hat{i})$ is the one way antenna gain function in the direction specified by the unit vector $\hat{i}$, $P_t$ is the transmitted power, R is the distance from the transmitter to the volume element in question, and $\langle \sigma_t(\hat{i}) \rangle$ is the average total scattering cross section of the scatterer. The line of integration is along the propagation of the wave, and the quantity $\gamma$ is the optical path length of the ray in question.

Throughout this report, angular brackets will indicate an average taken with respect to the distribution describing the scatterers.

If we ignore the contributions due to multiple incoherent scattering, then a simple radar equation approach gives the average received power $P_r$ from a given volume element dV as:

$$P_r = P_t \frac{\lambda^2}{(4\pi)^3} \frac{G_t(\hat{i})^2}{R^4} \rho \langle \sigma_b(\hat{i}) \rangle \exp(-2\gamma) dV \qquad 2.1.3$$

Here, $\langle \sigma_b(\hat{i}) \rangle$ is the average back scattering radar cross section of the scatterers, $\rho$ is the density of the scatterers, and $\lambda$ is the incident wavelength. Ishimaru refers to this approximation as First Order Multiple Scattering Theory. It is consistent with the first order approximation of the theory of Radiative Transfer, and the more rigorous Multiple Scattering Theory developed by Foldy and Twersky (Ishimaru 1978).

In terms of the field strength itself, the contribution to the returned signal of this volume element is a randomly phased sum of identically distributed scattering amplitude functions. Hence, by invoking the usual Central Limit Theorem argument, the scattering amplitude function of a given volume element can be represented by a zero mean complex Gaussian variable, whose mean power is given by Equation 2.1.3. Strictly speaking, this result is valid only for a finite volume element which contains enough scatterers for the Central Limit Theorem to be applicable; in practice, this means that we require that the integrals involved should be adequately approximated numerically by a sum over volume elements whose size satisfies this criteria.

A chaff cloud consists of a large number of randomly orientated resonant dipoles. The average back scattering cross section of randomly orientated dipoles has been the subject of much research. Detailed solutions for the boundary problem involved provide information concerning the width of the resonance peaks as it relates to the radius of the dipoles (see for example, Bowman et al. 1969). A simple approximation that is sufficient for our purposes, attributed to Chu (Van-Vleck et al. 1947), for the case of isotropically random half-wave dipoles illuminated by a linearly polarised wave is

$$\langle \sigma_b \rangle = (0.151)\lambda^2 \qquad 2.1.4$$

However, there does not appear to be published material available for total scattering cross section, $\langle \sigma_t \rangle$. This is evaluated in Appendix I according to the Chu resonance formulae, and we obtain the simple result for half-wave and full-wave isotropically random dipoles:

$$\langle \sigma_t \rangle = \frac{1}{2\pi}\lambda^2 = (.15915494\ldots)\lambda^2 \qquad 2.1.5$$

To quantify the effects of multiple scattering, we appeal to the theory of Radiative Transfer as applied to the case where the scatterers scatter isotropically, often known as the Milne Problem. According to various studies of the bistatic radar cross section of chaff, the co-polarised bistatic radar cross section varies by a factor of 4 for the case of isotropically random half-wave dipoles (Mack and Reiffen 1964), (Dedrick et al. 1978), (Peebles 1984). The solution of the Milne Problem can therefore act as a guide to the order of magnitude involved concerning multiple scattering. It can be shown that a series solution for the average intensity in the Milne Problem, whose terms have the physical interpretation of increasing orders of multiple scattering, converges according to the quantity:

$$1 - \exp(-\rho\sigma_t R_c) \approx \rho\sigma_t R_c + O((\rho\sigma_t R_c)^2) \qquad 2.1.6$$

Here, $R_c$ is some characteristic linear dimension of the cloud, such as the radius for a spherical cloud. Therefore, we require that $\rho\langle\sigma_t\rangle R_c$, the optical depth of the cloud, to be small compared to unity for First Order Multiple Scattering theory to be valid. If we interpret the quantity $(\rho\langle\sigma_t\rangle)^{-1}$ as the mean free

path for scattering (Ishimaru 1978), then this requirement translates to saying that the mean free path for scattering relative to the size of the cloud shall be large relative to unity. In Figure 1, the ratio of the mean free path for scattering to the radius of a spherical cloud is plotted, where the total number of dipoles is $10^8$. It can be seen that for a 50 m radius cloud that this ratio is much larger than unity, implying that multiple scattering is dominant. On the other hand, for a radius of 200 m, this ratio is much smaller than unity, implying that the effect of higher order multiple scattering can be neglected. According to Equation 2.1.6, multiple scattering effects in this case would be of the order of 10% of the total return.

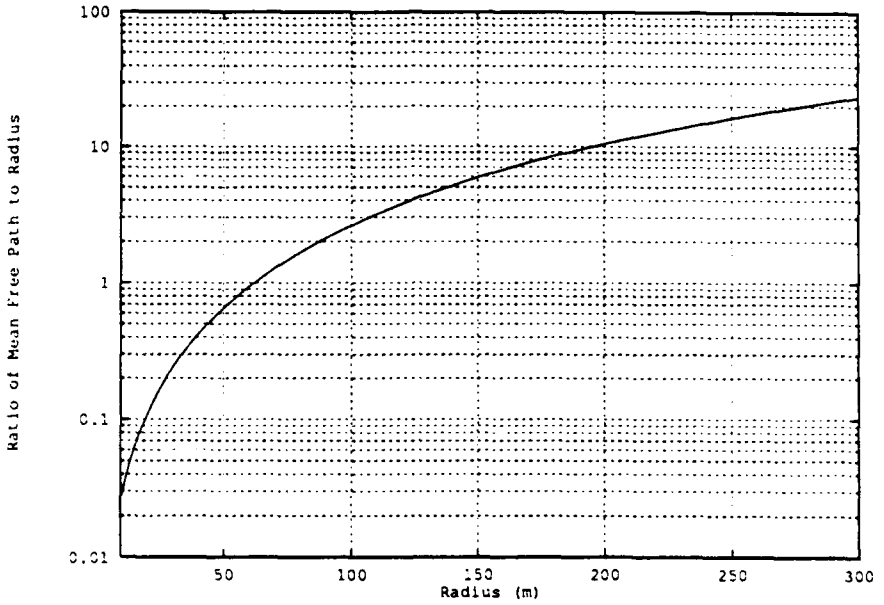


**Figure 1 The ratio of the mean free path for scattering to the radius of the chaff cloud, as a function of the radius of the chaff cloud.**

In this report, we shall consider a 200 m radius spherical cloud with $10^8$ dipoles, so that we can safely use the First Order Multiple Scattering Theory. The physical model for the scattering from a chaff cloud in this case is to assume each volume element of the chaff cloud is illuminated according to the attenuated power given by Equation 2.1.1, providing a mean power according to Equation 2.1.3, and has a scattering amplitude function which is a random sample from a zero mean Gaussian distribution which is statistically independent of the neighbouring volume elements.

## 2.2 Mathematical Derivation of Time Domain Return

The effect of a large number of independent scatterers upon the signal returned to a radar is often expressed in the form of a correlation function known as the two frequency correlation function (Ishimaru 1978), (Van-Trees 1971). For a distribution of stationary scatterers the two frequency correlation function reduces to the correlation function of a stationary random series. This type of target is known as a Range-Spread target (Van-Trees 1971), or a Wide Sense Stationary Uncorrelated Channel (WSSUC) (Ishimaru 1978). The essence of the simulation technique developed in this report is to obtain a sample path of this complex random series. From this we can obtain a random sample of the ensemble of possible radar returns from the chaff cloud. This we shall refer to as the chaff ensemble. The derivation is straightforward, following closely that of Van-Trees. It is included here to set notation, and indicates how we shall obtain and use the random series numerically. The reader who is concerned with mathematical rigour can verify that the following mathematical manipulations are valid for a narrow-band radar signal reflecting from a chaff cloud which is finite in size.

According to the physical model discussed above, each volume element scatters the incident wave once with a known delay to the receiver. Therefore the returned signal is a sum of overlapping echoes due to each volume element, modified by the scattering amplitude of the volume element and the relevant

propagation factors. This has the obvious mathematical form of a convolution integral. According to the discussion of the previous section, the scattering amplitude is a random sample of a zero mean complex Gaussian distribution, whose mean power can be calculated. Therefore, the field strength of the returned signal can be expressed formally by the stochastic integral in Equation 2.2.1.

$$s_o(t) = \int_{-\infty}^{\infty} s_i(t-t')\sqrt{\frac{c}{2}\Sigma(\frac{c}{2}t')}dZ(t') \qquad 2.2.1$$

Here, $s_i(t)$ is the complex envelope of the transmitted signal and $s_o(t)$ is the complex envelope of the received signal (all signals are treated according to the narrow band approximation), c is the speed of light, and Z(t) is a zero mean complex Gaussian process with orthogonal increments satisfying Equation 2.2.2:

$$\langle |dZ(t)|^2 \rangle = dt \qquad 2.2.2$$

The function $\Sigma(R)$, Equation 2.2.3, is the mean power scattered from all the scatterers within dR of the given range R:

$$\Sigma(R) = P_t \frac{\lambda^2}{(4\pi)^3} \int_A \frac{G_t(\hat{i})^2}{R^4} \rho\langle\sigma_b\rangle \exp(-2\gamma) dA \qquad 2.2.3$$

The ensemble average of the correlation in time of the received signal is therefore

$$\begin{aligned} \langle s_o(t_1)\overline{s_o(t_2)}\rangle &= \int_{-\infty}^{\infty} s_i(t_1-t)\overline{s_i(t_2-t)}\frac{c}{2}\Sigma(\frac{c}{2}t)dt \\ &= \int_{-\infty}^{\infty} s_i(t_1-\frac{2}{c}R)\overline{s_i(t_2-\frac{2}{c}R)}\Sigma(R)dR \end{aligned} \qquad 2.2.4$$

In particular, the ensemble average received power is the convolution integral:

$$\begin{aligned} \langle \frac{1}{2}|s_o(t_1)|^2 \rangle &= \int_{-\infty}^{\infty} \frac{1}{2}|s_i(t_1-t')|^2 \frac{c}{2}\Sigma(\frac{c}{2}t')dt' \\ &= \int_{-\infty}^{\infty} \frac{1}{2}\left|s_i(t_1-\frac{2}{c}R)\right|^2 \Sigma(R)dR \end{aligned} \qquad 2.2.5$$

The physical interpretation of Equation 2.2.5 is that the ensemble average of the received power envelope is the convolution of the transmitted power envelope and the scattering function $\Sigma(R)$.

The ensemble average of the correlation in frequency of the returned signal is given Equation 2.2.6, assuming that required change of order of integrations is valid.

$$\begin{aligned} \langle S_o(f_1)\overline{S_o(f_2)}\rangle &= S_i(f_1)\overline{S_i(f_2)} \int_{-\infty}^{\infty} \exp(-2\pi i (f_1-f_2)t)\frac{c}{2}\Sigma(\frac{c}{2}t)dt \\ &= S_i(f_1)\overline{S_i(f_2)}\Gamma(f_1-f_2) \end{aligned} \qquad 2.2.6$$

The function $\Gamma(f)$, the two frequency correlation function, represents the complex correlation function of a stationary complex random series in the frequency domain, which by construction is a zero mean complex Gaussian random series. We therefore represent the chaff cloud mathematically as a zero mean complex Gaussian random series in the frequency domain, whose spectral density is $(c/2)\Sigma(ct/2)$. Its spectral representation is given by Equation 2.2.7.

$$S_c(f) = \int_{-\infty}^{\infty} \exp(-2\pi i f t') \sqrt{\frac{c}{2}\Sigma(\frac{c}{2}t')}\, dZ(t') \qquad 2.2.7$$

We then define the Fourier transform of received signal by Equation 2.2.8, and obtain the received signal by Equation 2.2.9.

$$S_o(f) = S_i(f) S_c(f) \qquad 2.2.8$$

$$s_o(t) = \int_{-\infty}^{\infty} \exp(2\pi i f t) S_o(f)\, df \qquad 2.2.9$$

It can be verified that the received signal defined in this way satisfies Equations 2.2.4 and 2.2.6. The problem of obtaining a random sample of the time domain return from a chaff cloud is therefore reduced to obtaining a random sample of $S_c(f)$, Equation 2.2.7, and then evaluating the correlation integral via Equations 2.2.8 and 2.2.9.

## 2.3 Numerical Characteristics of Time Domain Return

We now examine the numerical implementation of the above calculations. We use the Discrete Fourier Transform (DFT) to numerically approximate the required Fourier Transformations, and so we must choose appropriate values for the total band width 2F, and the total time 2T, taking into account that the total number of points for the transform, N, is given by N=(2T)(2F). The DFT is implemented by a Fast Fourier Transform (FFT), so we also require that N be a power of two. The aim of the discussion is to select appropriate values for 2F and 2T such that the numerical calculations are reasonably faithful to the physical picture outlined above.

Although the discussion of Section 2.1 indicates that the contributions of the higher order scattering are about 10% relative to the approximate scattering theory we are using here, there is a need to calculate this approximate theory to a higher level of precision. We shall be performing many non-linear transformations upon the simulated signal, and we do not wish to allow spurious harmonics due to insufficient band limiting, or other defects in our numerical calculations, to interfere with the observations we wish to make. We are not justified in using a level of precision beyond $10^{-4}$ though, as at this point we may be going beyond the validity of the narrow-band approximation, upon which all of the above analysis depends. We therefore choose 2T and 2F so that the numerical errors in our calculations are about $10^{-4}$.

We use a sampling technique for a stationary correlated Gaussian series of known spectrum that is sometimes used in radar signal simulation (Mitchell 1976). The idea is to use a discrete approximation for the spectral representation of the random series, Equation 2.3.1.

$$S_c(n\delta f) = \sum_{m=0}^{N-1} \exp(-2\pi i \frac{nm}{N}) \left(\sqrt{\frac{c}{2}\Sigma(\frac{c}{2}m\delta t)}\right)^{\frac{1}{2}} (N(0,\delta t) + iN(0,\delta t)) \qquad 2.3.1$$

$$\Gamma_d(n\delta f) = \sum_{m=0}^{N-1} \exp(-2\pi i \frac{nm}{N}) (\frac{c}{2}\Sigma(\frac{c}{2}m\delta t))\, \delta t \qquad 2.3.2$$

Here, N(a,b) represents a randomly sampled real Gaussian variable, with mean a and variance b. It is easily shown this discrete form of the spectral representation of $S_c(f)$ provides a sequence of numbers whose correlation function, $\Gamma_d$ of Equation 2.3.2, is the DFT of the sampled spectral density. We position the cloud so that it is fully contained within the interval (0,T), so that the Fourier series in Equation 2.3.2 converges in the sense that extra terms contain no energy. However, the discrete correlation function $\Gamma_d$ is periodic with period 2T. Indeed, it is easy to show that the Fourier series is that of the infinite sum of $\Gamma(f)$ spaced 2T apart (an aliasing effect). To ensure that this effect is negligible to a level of $\varepsilon$, F must be sufficiently large such that $\Gamma(f)<\varepsilon$ for all $f<F$. In Appendix II it is shown that for a distant spherical cloud where multiple incoherent scattering can be ignored $\Sigma(R)$ is approximately

$$\Sigma(R+z) \approx P_0 \rho \langle \sigma_b \rangle (R_c^2 - z^2) \qquad \text{for } |z| \le R_c \tag{2.3.3}$$

In this approximation, the two frequency correlation function is given by Equation 2.3.4, where $j_1(x)$ is the Spherical Bessel function of order 1.

$$\Gamma(f) = |S_c(f)|^2 = P_0 \rho \langle \sigma_b \rangle (4\pi R_c^3) \left( \frac{j_1(\mu)}{\mu} \right) \qquad \text{where} \mu = 2\pi f \left( \frac{2R_c}{c} \right) \tag{2.3.4}$$

For $\mu$ large relative to unity,

$$\varepsilon \sim \left| -\frac{3}{\mu^2} \cos\mu \right| \le \frac{3}{\mu^2} = \frac{3}{4\pi^2} \left( \frac{c}{2R_c} \right)^2 \frac{1}{f^2} \tag{2.3.5}$$

Therefore, we choose F by Equation 2.3.5, on the understanding that the resulting choice for F renders $\mu$ large relative to unity.

$$F = \frac{\sqrt{3}}{2\pi} \left( \frac{c}{2R_c} \right) \frac{1}{\sqrt{\varepsilon}} \tag{2.3.6}$$

If, for example, $R_c$ is 200 m and $\varepsilon$ is $10^{-4}$, then F is 20.7 MHz and the time step that this implies is 24.2 ns, or 3.6 m in radar length. From the point of view of ensuring that each volume element in the discrete approximation contains a reasonable number of scatterers, so that the Central Limit Theorem is valid, this is a reasonable value.

We now consider the evaluation of the correlation integral in Equation 2.2.10. For a pulsed radar, the spectral density of the transmitted signal, $|S_i(f)|^2$, is given by Equation 2.3.7.

$$|S_i(f)|^2 = 2P_t\tau^2 \left( \frac{\sin\pi f\tau}{\pi f\tau} \right)^2 \le 2P_t\tau^2 \frac{1}{(\pi f\tau)^2} \tag{2.3.7}$$

The radar will employ a matched filter, which will further improve the band limiting behaviour of this signal. We shall use the single pole approximation, Equation 2.3.8, in our calculation (Skolnik 1981). The filter has been normalised to preserve the DC levels.

$$S_m(f) = (1 - 2\pi i f\tau)^{-1} \tag{2.3.8}$$

In this case, Equation 2.2.8 becomes:

$$S_o(f) = S_c(f) S_i(f) S_m(f) \tag{2.3.9}$$

The ratio of the ensemble average of the spectral density of the received signal for large frequency values

to its value at the origin is:

$$\frac{\langle|S_o(f)|^2\rangle}{\langle|S_c(0)|^2\rangle} = \left(\frac{\sin\pi f\tau}{\pi f\tau}\right)^2 \frac{1}{|1-2\pi i f\tau|^2} < \frac{4}{(2\pi f\tau)^4} \equiv \varepsilon \qquad 2.3.10$$

To maintain the desired level of band limiting on the received signal power to the level of precision ε, we should choose the total band width F by

$$F = \frac{1}{\pi\sqrt{2}}\frac{1}{\tau}\sqrt[4]{\frac{1}{\varepsilon}} \qquad 2.3.11$$

If we use a pulse width of 0.1 μs, and set ε to $10^{-4}$, then the band width given by this formula is 22.5 MHz and the time step implied by this choice is 22.2 ns, or 3.4 m in radar length. This is about the same value as that required for the sampling of the random series representing the cloud.

In our simulations we shall need to include the effect of wide band noise passing through the matched filter. When examining the action of the range discriminant, or the output of a logarithmic detector, this will prevent unphysical divisions by zero, or similar numerical problems occurring, by providing a physically plausible noise floor. We shall refer to a sample of this signal as a sample from the thermal ensemble. This signal will change on a pulse by pulse basis, unlike the chaff signal which will evolve over a period of a large number of pulses. We can obtain a random sample of this signal in a similar fashion as that used for the chaff cloud. The average of the spectral density over the thermal ensemble of this signal is

$$|S(f)|^2 = \frac{kT_s}{|1-2\pi i f\tau|^2} < \frac{1}{4\pi^2}\frac{kT_s}{(f\tau)^2} \equiv \varepsilon \qquad 2.3.12$$

Here, k is Boltzmann's constant, and $T_s$ is the system temperature of the radar receiver. If we select F according to Equation 2.3.11, then Equation 2.3.12 becomes

$$\frac{|S(F)|^2}{|S(0)|^2} \approx \frac{\sqrt{\varepsilon}}{2} \qquad 2.3.13$$

If ε is $10^{-4}$, then the band limiting according to Equation 2.3.13 will be 5 $10^{-3}$. In general, the signal power of the wide band noise through the matched filter will be small compared to the return from the chaff cloud, allowing us to tolerate this reduced level of accuracy.

Having chosen an appropriate value for the total band width 2F, we now examine the selection of the total time interval 2T. The interval (0,T) should contain the entire return from the chaff cloud. It is therefore set by the diameter of the sphere in radar time, $2(2R_c/c)$, plus some multiple of the pulse width τ. Since the rate of decay of the output of the matched filter used here is $\exp(-(t-\tau)/\tau)$, we choose this multiple of τ to be 12, so that the chaff return will be fully contained within a time interval of T to a level of $10^{-4}$. This also reduces the error introduced by aliasing of the matched filtered signal to about $10^{-4}$.

In general, we shall pick the larger of the two values provided by Equations 2.3.5 and 2.3.11 for F, using the value of T discussed above. To obtain a power of two for N, we increase F as required. In the simulations carried out in this report, we use a set of conditions which are typical of those encountered by an ASM. To prevent repetition, we state the conditions here. The radar is a pulsed radar with a carrier frequency of 9.45 GHz, with 40 kW of peak power, a one way antenna gain of 30db, and with a system temperature of 1000 K. Typically, the PRF will be of the order of kHz. We use a spherical cloud of radius 200 m, with $10^8$ isotropically aligned dipoles, and its centre is at a range of 10 km. With this geometry, the cloud will be fully contained within the 3dB beam width of the antenna pattern. The pulse width of the radar will be either 0.1 μs or 0.5 μs, which implies that we should use 512 and 1024 points respectively for the FFT.

# 3 SIMULATIONS CONCERNING THE PERCEIVED RCS OF A CHAFF CLOUD

The essential reason for developing the simulation technique of this report is to obtain direct data concerning the effect of this type of return upon the range discriminant of a range tracking radar. In this section we discuss a by-product of this analysis, the perceived RCS of a chaff cloud. We treat the average value of the power envelope of the return analytically. From this, we can also obtain analytical results for the RCS profile for a square law detector, linear and logarithmic detectors, and for a first order AGC loop driven by a linear detector. By comparing the average over the chaff ensemble from our simulations to the analytical results, we check the validity of the simulations.

## 3.1 RCS of a Chaff Cloud, as Perceived by a Square Law Detector

One method of assessing the RCS of the chaff cloud is to use the integrated cross section, which is simply the total power returned by the cloud relative to the power returned by a point target of known radar cross section held at the same range. This is the RCS that would be appropriate to use for a continuous wave radar (CW), and is given by Equation 3.1.1.

$$\sigma_{cw} = \frac{1}{P_0}\int \Sigma(R)dR \qquad 3.1.1$$

Here, $P_0$ is the power returned by a steady point target held at the same range. Explicit expressions for the CW RCS for a distant spherical cloud are derived in Appendix II. In the limit of small optical depth these expressions reduce to the sum of the power returned from each scatterer. For example, a cloud of $10^8$ isotropically randomly orientated dipoles and a carrier frequency of 9.45 GHz the CW RCS is 14740 $m^2$.

For a pulsed radar, the notion of CW RCS applies only where the pulse length is large relative to the dimensions of the chaff cloud. Many ASMs use a pulse width of the order of 0.1 μs (radar pulse length of 15 m). Therefore, the concept of CW RCS is not an appropriate measure of the signal power returned by the chaff cloud for these ASMs; that is, we must take into account the dimensions of the chaff cloud. This is often taken into account by the Radar Resolution Method where the power seen by the radar is approximated by the sum of the power returned by the scatterers contained in the volume element resolution cell of the radar system (see for example, Schleher 1986). This is a crude version of the power envelope of the chaff return as found by the convolution integral of Equation 2.2.5. In this report we shall relate the power envelope of the return as calculated by the correlation integral to that obtained from simulations, according to various detectors. For a point target, the RCS can be judged by the peak output of the matched filter. Therefore, the power envelope of the cloud in our simulations will be calibrated against the peak value of the power envelope of a point target held at the same range. In this sense we can obtain a RCS profile of the chaff cloud which could be verified experimentally.

The signal presented to the radar detector is a mixture of the chaff return, and the filtered thermal noise. The thermal noise varies on a pulse by pulse basis, but the chaff return evolves on a much slower time scale, consisting of a large number of pulses. In principle, we should average over the thermal ensemble before obtaining the average over the chaff ensemble. However, in the calculations performed in this section we note that the chaff signal power completely dominates over the thermal noise power in the central portion of the chaff return, which is what we are interested in here. Hence, for the purposes of obtaining estimates of the chaff signal power as perceived by the detector in question, we can ignore the distinction between the time scales of these two signals.

In Figure 2, a typical simulation of the output of a matched filter according to a square law detector is shown; the smooth curve is the ensemble average from Equation 2.2.5. In this example we have used a pulse width is 0.1 μs. The vertical scale has been scaled so that unity is the peak output from a point target of unit radar cross section. Hence we may interpret the vertical scale as the RCS profile as discussed above. Clearly, a given sample of the time domain signal from the cloud, as calculated by the technique developed in this report, consists of many peaks and in no way resembles the ensemble average signal calculated by the convolution integral of Equation 2.2.5. Figure 3 shows the average taken over 1000 independent samples of the same return, and it is converging to the convolution integral as expected (the sample shown in Figure 2 was one of the samples used in calculating this average). The highest value of the RCS profile

according to the convolution integral (see Figure 3) is about 770 $m^2$, whereas the CW RCS of this cloud is 14740 $m^2$, representing a loss of 12.8dB relative to the CW RCS of the cloud.

We repeat this analysis for a radar whose pulse width is 0.5 μs. We would expect that for these dimensions that the perceived RCS profile would be larger, as the pulse length relative to the size of the cloud is larger. Indeed, this is the case. Figure 4 shows a random sample of the return from the cloud superimposed upon the result calculated from the convolution integral. Again, a single random sample of the return is composed of many peaks, and does not resemble the smooth result available from the convolution integral.

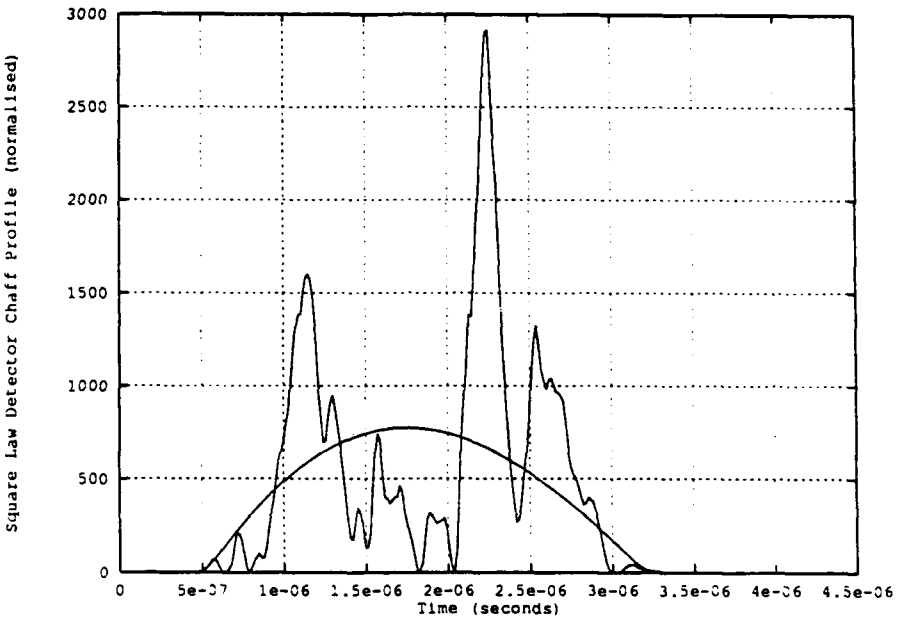


**Figure 2 The RCS profile of the chaff cloud for the square law detector, using the 0.1 μs radar. The smooth curve is the ensemble average, and the spiky curve is a random sample.**

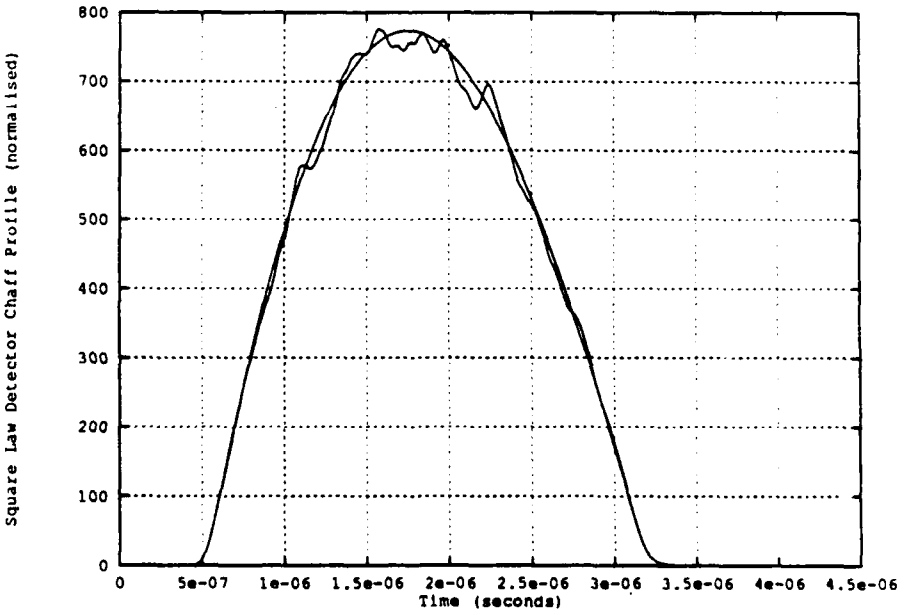


**Figure 3 The average over 1000 samples of the received signal for the square law detector, using the 0.1 μs radar. The maximum ensemble average RCS obtained is 770 $m^2$.**

Figure 5 is the average result of 1000 independent random samples superimposed upon the convolution result (the smooth curve). The highest value of the RCS profile in this case is 3400 $m^2$, a loss of 6.4dB relative to the CW RCS of the cloud.

In conclusion, the average RCS profile obtained from simulations agrees well with the analytical result obtained from the convolution integral. Individual random samples of the RCS profile in no way resemble the shape of the RCS profile obtained from the convolution integral. The RCS as perceived by the radars considered here reflects the size of the pulse length relative to the dimensions of the cloud, as we would expect.

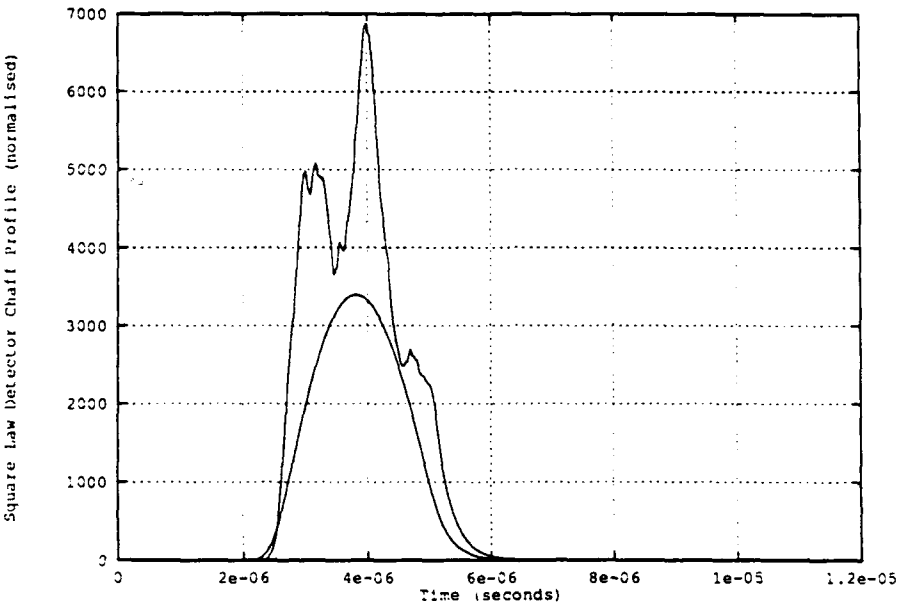


**Figure 4 The RCS profile of the chaff cloud for the square law detector, using the 0.5 μs radar. The smooth curve is the ensemble average, and the spiky curve is a random sample.**

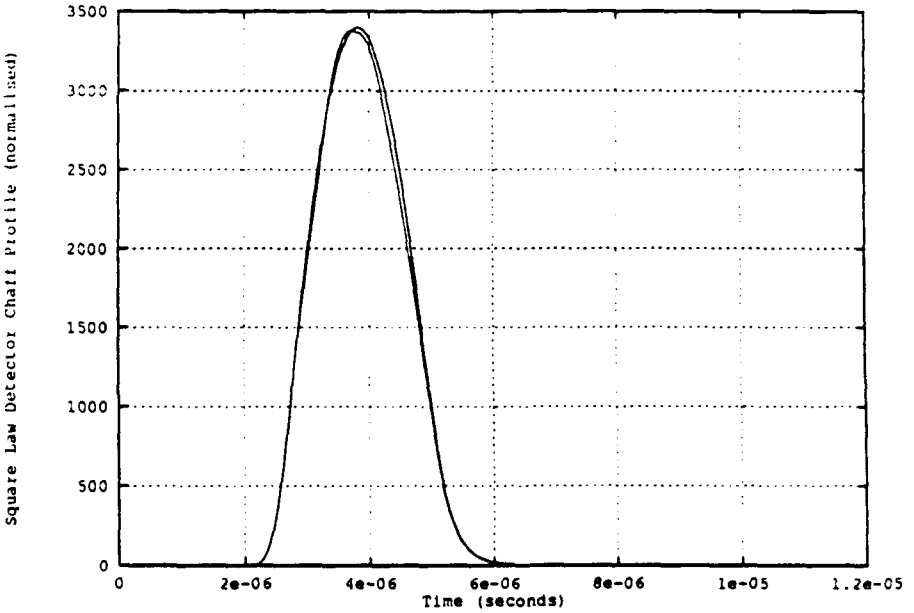


**Figure 5 The average over 1000 samples for the square law detector of the received signal, using the 0.5 μs radar. The maximum ensemble average RCS obtained is 3400 $m^2$.**

## 3.2 RCS of a Chaff Cloud, as Perceived by a Linear and Logarithmic Detector

Since the chaff return is a zero mean complex Gaussian process, we can use the ensemble average power to obtain the average over the chaff ensemble for a linear envelope detector, Equation 3.2.1, and a logarithmic detector, Equation 3.2.2 ($\gamma$=0.57721566... is Euler's constant) (see for example, Deutsch 1962).

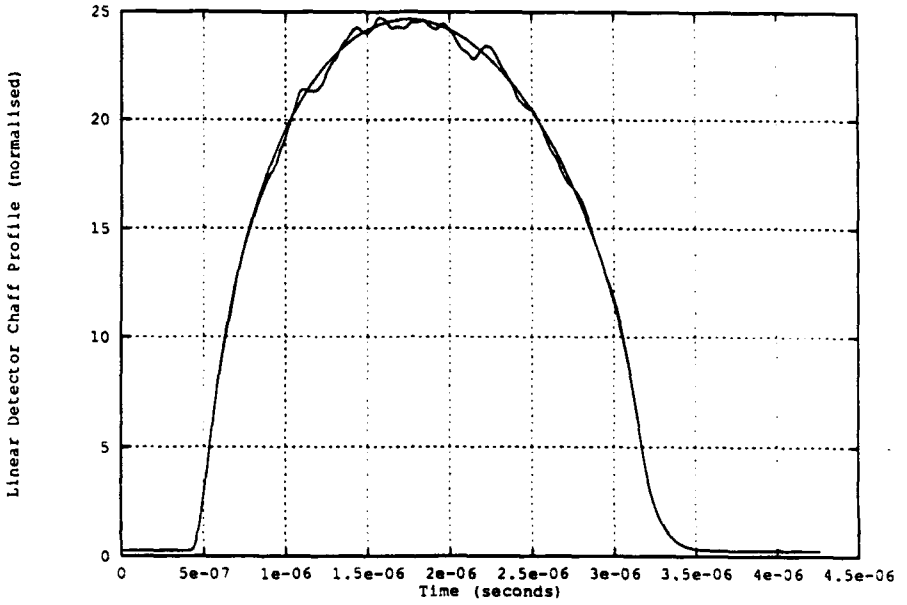


**Figure 6 The average over 1000 samples for the linear detector of the received signal using the 0.1 μs radar. The maximum ensemble average RCS obtained is 580 $m^2$.**

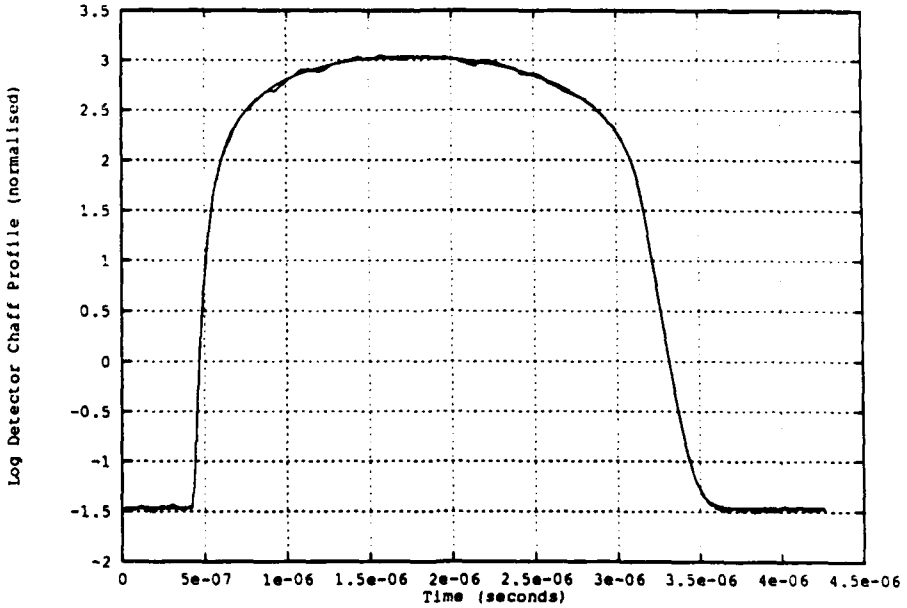


**Figure 7 The average over 1000 samples for the log detector of the received signal, using the 0.1 μs radar. The maximum ensemble average RCS obtained is 400 $m^2$.**

$$\langle |s_o(t)| \rangle = \sqrt{\pi} \sqrt{\langle \frac{1}{2} |s_o(t)|^2 \rangle} \qquad 3.2.1$$

$$\langle \log |s_o(t)| \rangle = \frac{1}{2}(-\gamma + \log 2) + \frac{1}{2} \log \langle \frac{1}{2} |s_o(t)|^2 \rangle \qquad 3.2.2$$

As these detectors are memoryless transformations of the signal, the ragged nature of a single random sample of the cloud's return can be inferred from the examples given above. We shall only display a comparison of the average obtained from the simulations to the values obtained from the analytical results. Figure 6 shows the average of 1000 independent random samples obtained from simulations superimposed upon analytical result (smooth curve) for a linear detector, while Figure 7 gives the results obtained for a logarithmic detector. Both of these sets of results are for a pulse width of 0.1 μs, and the vertical scale in each case has been scaled so that unity corresponds to the response obtained from a steady point target with unit RCS held at the same range. In both cases the agreement between the analytical result and the simulations is excellent.

From these profiles we may obtain the average RCS as perceived by these systems relative to a steady point target of known RCS and range. For the linear detector, we have 580 $m^2$, and for the logarithmic detector 400 $m^2$. These values are a bit smaller than that obtained from the square law detector (770 $m^2$), representing a loss of 14.0dB and 15.7dB respectively relative to the CW RCS of the cloud. For the simulations for a 0.5 μs pulse width, the agreement between the simulations and the analytical result is of the same quality. The maximum average RCS achieved for the linear detector was 2700 $m^2$, and for the logarithmic detector was 1600 $m^2$, representing a loss of 7.4dB and 9.6dB respectively relative to the CW RCS of the cloud.

In view of the fluctuating nature of the return from a chaff cloud, these average values represent only typical values of the strongest part of the clouds RCS profile. Nevertheless, the losses are of the order of 15dB relative to the CW RCS value of 14740 $m^2$ for the 0.1 μs pulse width, and 8dB for the 0.5 μs pulse width. These values are consistent with the relative size of the pulse length to the dimensions of the cloud.

## 3.3 RCS of a Chaff Cloud, as Perceived by an AGC Loop

Pulsed radar systems often employ an AGC loop driven by a linear envelope detector. This class of circuit has been analysed in the literature, and we shall consider here a simplified model for this circuit due to Ohlson (1974). With reference to the schematic diagram in Figure 8 the following set of formulae describe the operation of the First Order AGC loop.

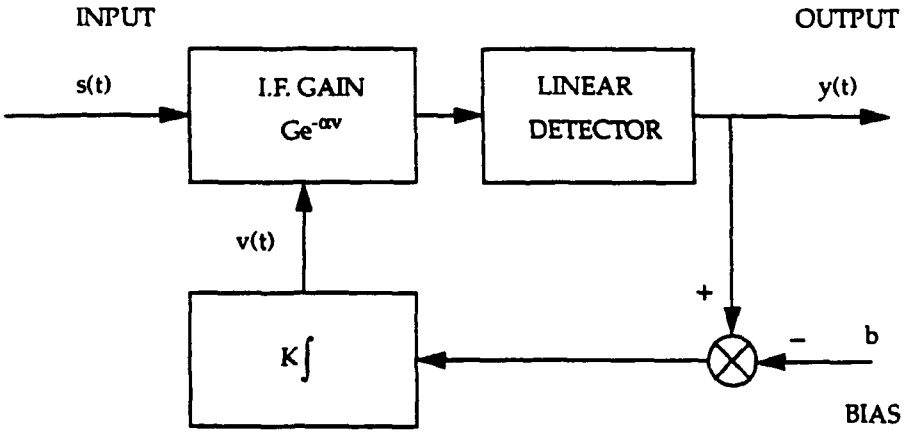


**Figure 8 First order AGC loop block diagram.**

$$v(t) = C + \log\left(h \otimes |s|(t)\right) \tag{3.3.1}$$

$$y(t) = b\frac{|s|(t)}{h \otimes |s|(t)} \tag{3.3.2}$$

$$C = \frac{1}{\alpha}\log\frac{G}{b} \tag{3.3.3}$$

$$h \otimes |s|(t) = \int_{-\infty}^{t} \frac{1}{\beta}\exp(-(t-\xi)/\beta)|s(\xi)|\,d\xi \tag{3.3.4}$$

$$\beta = \frac{1}{K\alpha b} \tag{3.3.5}$$

Here, s(t) is the signal in complex envelope form, y(t) is the output, v(t) is the control voltage, G and $\alpha$ define the exponential gain characteristic curve of the amplifier, K is the gain of the integrating element, b is the bias voltage, and $\beta$ is the AGC time constant.

In practice, it is the control voltage v(t) which is accessible to the experimentalist, and from which the perceived RCS of the target is deduced. This in turn is a logarithmic transformation of the convolution integral of Equation 3.3.4. Thus, the key quantity to evaluate is the convolution integral, which we shall adopt as our measure of the signal. However, we are forced to consider the effect of thermal noise in evaluating this convolution integral, since it appears in the denominator of Equation 3.3.2. Due to the integrating action of the AGC circuit, we should expect some averaging with respect to the thermal ensemble for a given sample of the chaff ensemble in the evaluation of this convolution integral.

We shall examine this point in more detail. The signal is pulsed, and we shall assume that the PRI is large relative to the AGC time constant $\beta$, but small relative to the correlation time of the chaff return. Also, we shall assume that the signal provided to the AGC loop is gated and that the gate width is small in comparison to the AGC time constant $\beta$. Under these conditions, the convolution integral degenerates into a discrete First Order filter, driven by the integral of the linearly detected sum of the chaff return and the thermal noise over the selection gate, Equation 3.3.6. Here, $T_p$=1/PRF is the pulse repetition time.

$$h \otimes |s|(t) \approx X = \sum_{m=-\infty}^{n} \frac{1}{\beta}\exp(-(n-m)\,(T_p/\beta))X_m$$
$$X_m = \int_{m'\text{th gate}} |s(t)|\,dt \tag{3.3.6}$$

Considering that the AGC time constant $\beta$ is considerably shorter than the time scale describing the time evolution of the chaff return, we see that the convolution integral will be well approximated by its mean value over the thermal ensemble while holding the chaff return constant, Equation 3.3.7. The Rice function used in Equation 3.3.7 is the well known mean value for the Rician probability distribution for of a steady signal of amplitude A corrupted by complex Gaussian noise with a noise power of $N_0$ (Rice 1944).

$$X = \frac{1}{\beta\left(1-e^{-1/\beta}\right)}\int_{\text{gate}} \text{Rice}(|s_o(t)|, N_0/(2\tau))dt$$
$$\text{Rice}(A, N_0) = \sqrt{2N_0}\frac{\sqrt{\pi}}{2}\,{}_1F_1\left(-\frac{1}{2};1;-\frac{A^2}{2N_0}\right) \tag{3.3.7}$$

This integral can be written as a correlation integral by using a gate function g(t), Equation 3.3.8, which

allows us to examine the control voltage as we place the selection gate in different positions relative to the cloud return. Here, g(t) is unity over the width of the selection gate, and zero elsewhere. For our simulated chaff return, this integral can be implemented numerically by a FFT.

$$X = X(t_g) = \frac{1}{\beta(1-e^{-1/\beta})}\int_{-\infty}^{\infty} g(t-t_g)\,\mathrm{Rice}(|s_o(t)|, N_0/(2\tau))dt \qquad 3.3.8$$

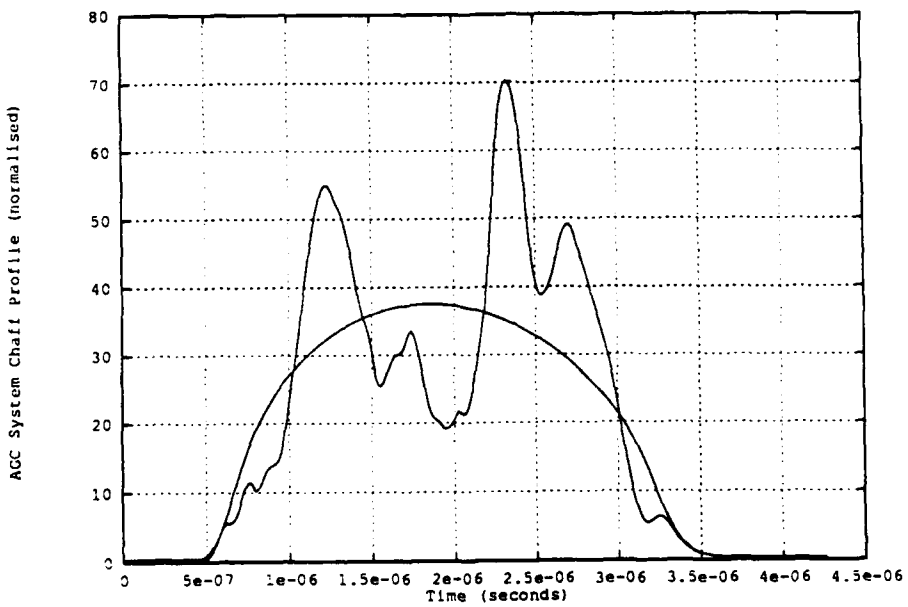


**Figure 9 The RCS profile of the chaff cloud for the AGC system, using the 0.1 μs radar. The smooth curve is the ensemble average, and the spiky curve is a random sample.**

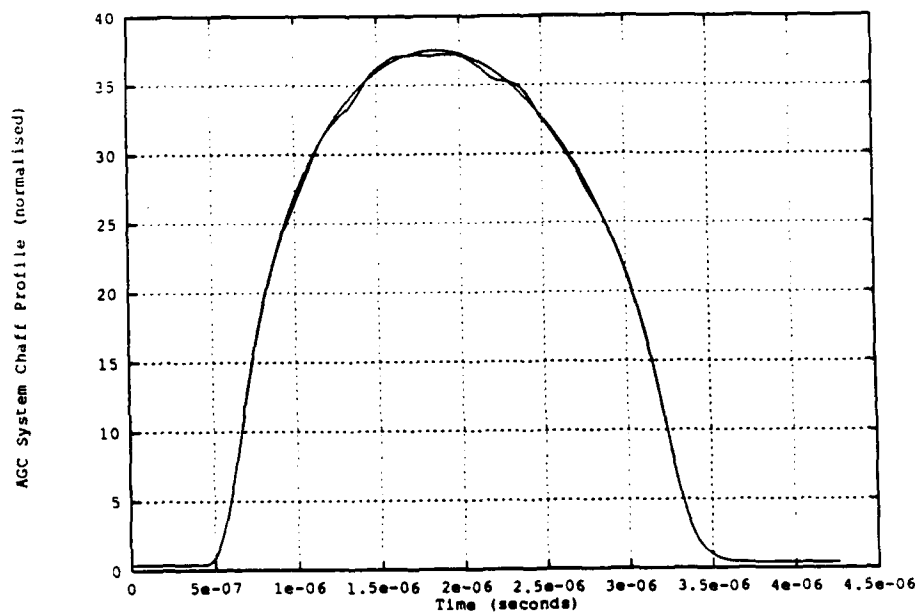


**Figure 10 The average over 1000 samples for the AGC system of the received signal, using the 0.1 μs radar. The maximum ensemble average RCS obtained is 1400 $m^2$.**

In Figure 9, the function $X(t_g)$ derived form the return displayed in Figure 2 is shown superimposed upon the analytical result of Equation 3.3.8; the vertical scale has been normalised by the peak output of a point target of unit RCS at the same range, under high signal to noise conditions. The AGC selection gate is 0.2 μs, or 2.0 pulse widths. The overall appearance of the sampled function is smoother than that of Figure 2. Figure 10 shows an average over the same 1000 samples used to generate Figure 3, superimposed upon the analytical result. The agreement is excellent, and the maximum value of the profile corresponds to a RCS of 1400 $m^2$, representing a loss of 10.2dB relative to the CW RCS of the cloud.

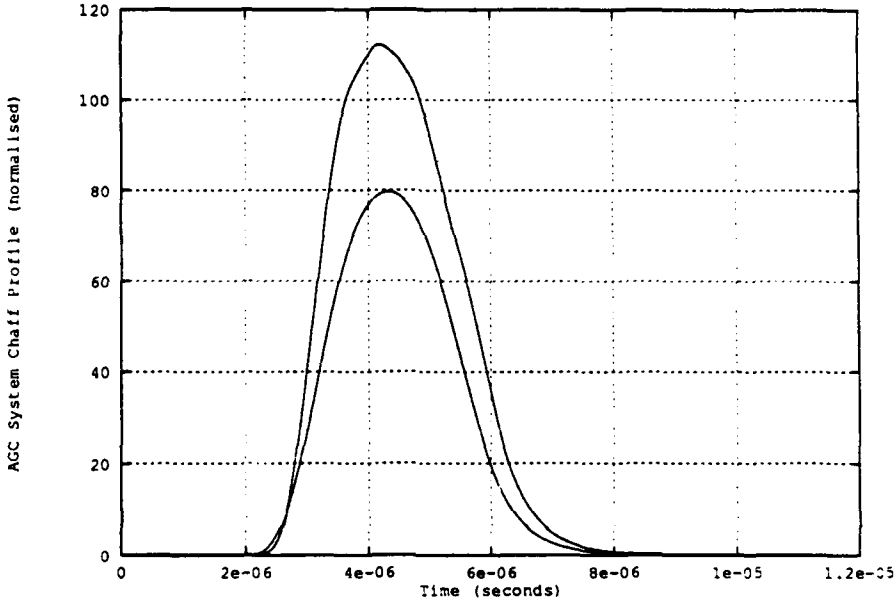


**Figure 11 The RCS profile of the chaff cloud for the AGC system, using the 0.5 μs radar. The small curve is the ensemble average, and the large curve is a random sample.**

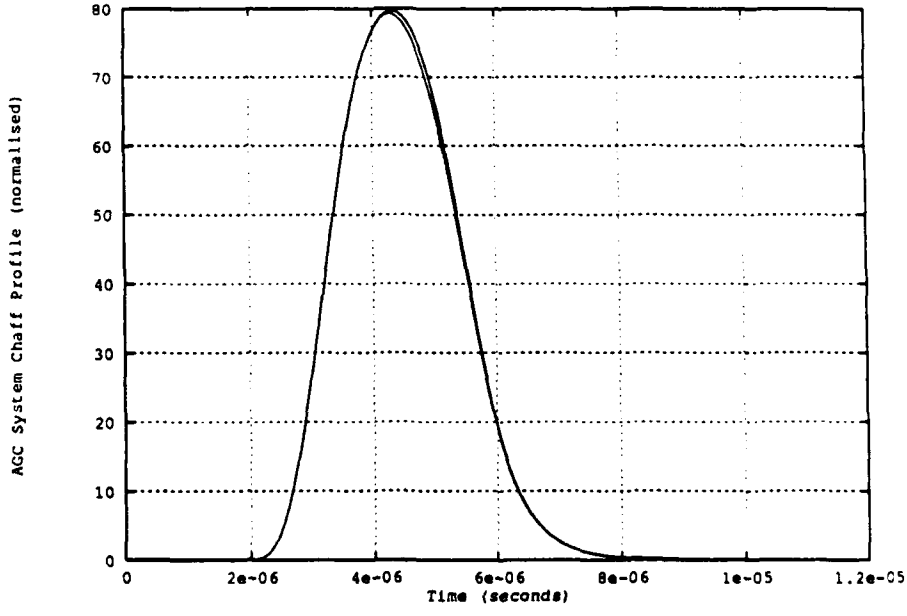


**Figure 12 The average over 1000 samples of the received signal for the AGC system, using the 0.5 μs radar. The maximum ensemble average RCS obtained is 1400 $m^2$.**

Figure 11 shows a random sample of the function $X(t_g)$ for a 0.5 μs pulse width, superimposed upon the analytical result. The AGC selection gate is 1.0 μs, or 2.0 pulse widths. Figure 12 is the average of 1000 independent samples superimposed upon the analytical result. The agreement is also excellent. The maximum value of this profile corresponds to a RCS of 6400 $m^2$, representing a loss of 3.6dB relative to the CW RCS of the cloud.

The larger values of the RCS as judged by the profile given here relative to those obtained for the square law, linear or log detectors probably stem from the width of the AGC selection gate (two pulse widths). Indeed, we find that the average values obtained here for a system employing AGC is approximately twice that obtained from the square law detector, reflecting the width of the AGC selection gate.

# 4 SIMULATIONS CONCERNING THE RANGE DISCRIMINANT

If we are to determine whether a given radar is able to track a chaff cloud in range, then the effect of the chaff return upon the range tracking loop needs to be examined. Generally, we cannot obtain analytical results due to the non-linear nature of the range discriminant, and so we must rely upon simulations to obtain the statistical characteristics of the range discriminant. The range discriminant which we examine here is a split gate discriminant, which is fed into a first order filter to smooth out the effects of thermal noise. Thus, we must carefully distinguish between averaging over the thermal ensemble, as performed by the low-pass filter described here, and averaging over the chaff ensemble which we perform to obtain the statistical characteristics of the chaff cloud as perceived by the range discriminant. In this way we obtain the average value of the range discriminant, its variance, and the correlation coefficient between the early and late gates of the range discriminant by a straightforward Monte-Carlo sampling analysis.

## 4.1 Range Discriminant with an AGC Loop

A range tracking loop is typically a feedback mechanism, with an error signal generated by some form of range discriminant. Often, an early-late gate system is employed, where the signal is passed through two gates, the early and late gates, integrated, and their difference found. If the signal has been normalised via the action of the AGC loop, an error signal which is largely independent of the strength of the signal is generated. Consistent with our previous notation, we define the functions e(t), l(t) to be unity within the range tracking selection gates, and zero elsewhere. The range discriminant, apart from some arbitrary multiplicative constant, is then given by Equation 4.1.1. In our simulation program, these correlation integrals are implemented via a FFT.

$$r(t_g) = \frac{\int_{-\infty}^{\infty} e(t-t_g)|s_o(t)|\,dt - \int_{-\infty}^{\infty} l(t-t_g)|s_o(t)|\,dt}{X(t_g)} \qquad 4.1.1$$

Here, $X(t_g)$ is taken from Equation 3.3.8, and is already averaged over the thermal ensemble as discussed in the previous section. This correlation integral provides us with a single sample of the chaff ensemble corrupted by a single sample from the thermal ensemble. The division by $X(t_g)$ in Equation 4.1.1 prevents the development of analytical expressions for the average value of the range discriminant.

This signal is then integrated by a low-pass filter, whose main purpose is to smooth out the fluctuations due to the thermal noise. The sole reason for including the effect of thermal noise at all in these simulations is to prevent numerical problems that would occur if it were removed. Therefore, the precise form of the filtering action discussed here is not critical for our analysis. The main requirements we place upon the filtering action are that it must be physically possible, and not disturb the operation of the radar system unduly. Hence, we shall model this low-pass filter by a first order discrete filter, Equation 4.1.2, where $r_m(t_g)$ is the m'th sample with respect to the thermal ensemble of the range discriminant of Equation 4.1.1, for a given sample from the chaff ensemble.

$$\begin{aligned} R_{n+1}(t_g) &= \exp(-1/\beta_r)R_n(t_g) + (1-\exp(-1/\beta_r))\,r_n(t_g) \\ &= (1-\exp(-1/\beta_r)) \sum_{m=-\infty}^{n} \exp(-(n-m)/\beta_r) r_m(t_g) \end{aligned} \qquad 4.1.2$$

In selecting a suitable value for $\beta_r$, we do not wish it to be too large, or else the response time of the filtered range discriminant will be too sluggish. However, we would like it to be sufficiently large so as to filter out the pulse to pulse variations due to the thermal noise. If we hold the chaff return constant over the period

of operation of the filter, we find that the variance of the filtered output is:

$$V[R_{n+1}(t_g)] = \frac{(1-\exp(-1/\beta_r))^2}{(1-\exp(-2/\beta_r))} V[r(t_g)]$$

$$\approx \frac{1}{2\beta_r} V[r(t_g)] \qquad \text{for } (\beta_r \gg 1) \qquad 4.1.3$$

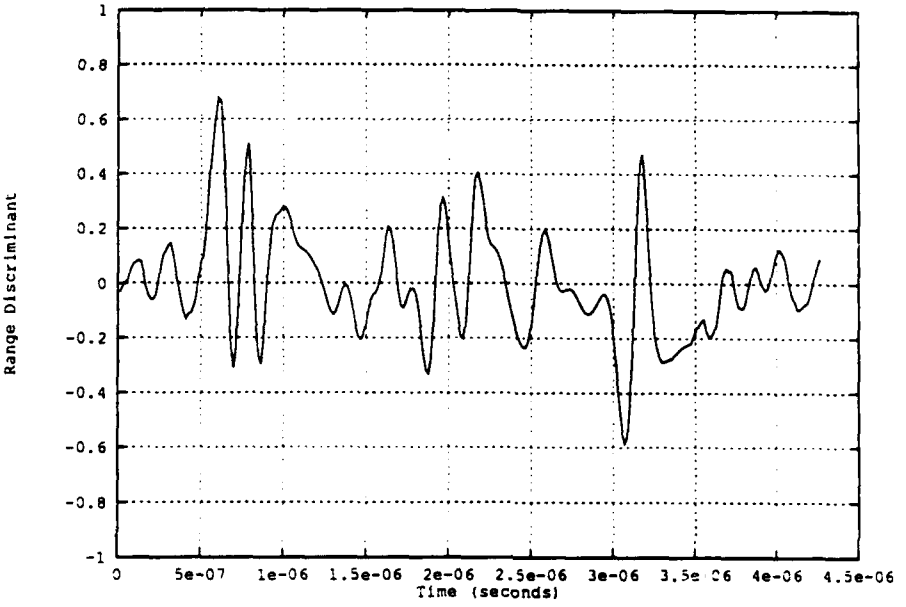


**Figure 13 A random sample of the range discriminant for the AGC system, using a 0.1 μs pulse width.**

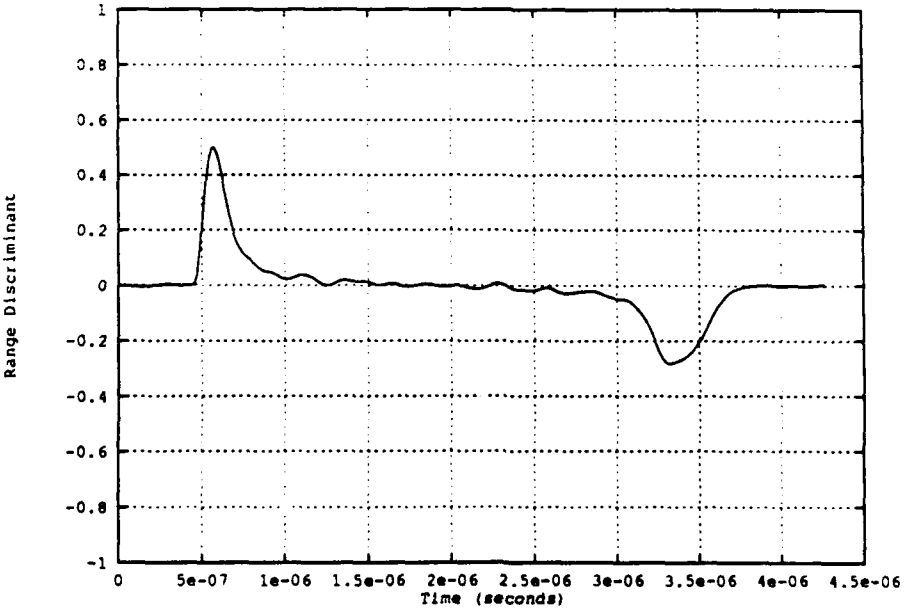


**Figure 14 The average over 1000 samples of the range discriminant for the AGC system, using a 0.1 μs pulse width.**

For a pulsed radar with a PRF of the order of kHz, we see that choosing $\beta_r$ to be 10 ensures that band width of the information provided to the remainder of the tracking loop is still well in excess of 10 Hz, and provides a reduction by a factor of 20 in the variance of the range discriminant. This is the value we choose for our simulations. We must also truncate the operation of the filter. If we use only N terms in the recurrence relation, then the variance given in Equation 4.1.3 is modified by a factor of $(1-\exp(-2N/\beta_r))$. Therefore, for numerical calculations we shall use N=10, implying that this factor is 0.865. Since the principal purpose for including thermal noise in our calculations at all is to provide numerical stability in

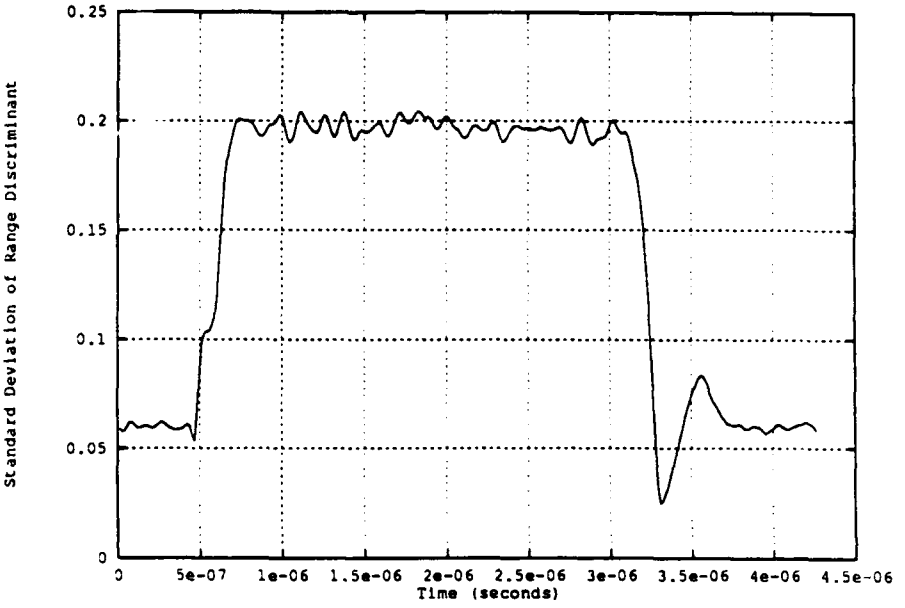


**Figure 15 The standard deviation of the range discriminant for the AGC system, using a 0.1 μs pulse width.**

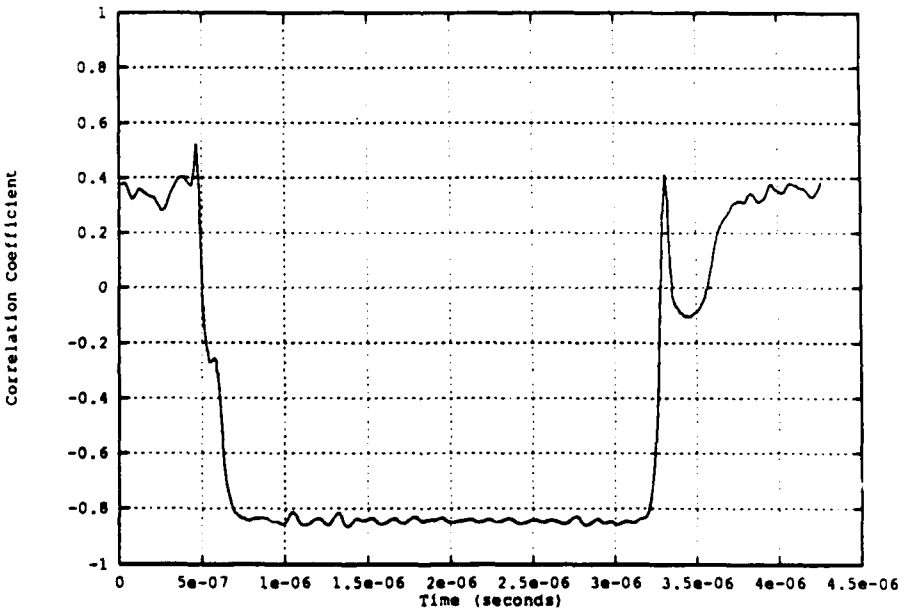


**Figure 16 The correlation coefficient of the early and late gates for the AGC system, using a 0.1 μs pulse width.**

a physically plausible way, this will be sufficient for our purposes.

For a 0.1 μs pulsed radar with selection gates of 0.08 μs width, a typical sample of range discriminant is shown in Figure 13; the average response over 1000 samples in Figure 14, and the standard deviation in Figure 15.

The average value has the behaviour that we would expect, in that it is close to zero outside the cloud and in the middle of the cloud, but has large peaks of the appropriate sign at the edges of the cloud. However, this structure which is clearly visible in Figure 14 is not at all apparent in the random sample of this process shown in Figure 13. The variance of the range discriminant shown in Figure 15 shows that within the cloud the standard deviation of the range discriminant is uniform, with a value of 0.2; the small fluctuations observed in this figure can be attributed to sampling fluctuations. On the trailing edge of there is a dip followed by a small rise, before the standard deviation settles back to the thermal noise value.

Another set of statistics that we can use to examine the behaviour of the range discriminant is the correlation of the outputs of the early and late gates; in particular, the correlation coefficient of these outputs. Again, this cannot be obtained analytically, and so we must rely upon simulations. We must be careful in analysing the statistical data to obtain the correlation coefficien., or some measure of the correlation of the early and late gates. It is well known that the Pearson Correlation Coefficient is useful only for data which is 'close' to the Gaussian form that it assumes (Press et al., 1986). We should therefore compare the results from this test to that from some of the non-parametric test such as the Spearman Rank-Order test, or the Kendall's Tau test. However, these non-parametric tests rely upon ordering the data, or some operation that requires that all of the data points to be held in memory, whereas the Pearson Correlation Coefficient can be obtained from a running sum, just as the sample mean and sample variance are obtained. From a programming point of view, we simply run out of computer memory. Hence, we shall use the Pearson Correlation coefficient to obtain data for each of the computed points, as was done for the sample mean and sample variance discussed elsewhere. We then identify some typical points and some unusual points, and examine their full statistics in more detail separately.

A graph of the Pearson Correlation Coefficient of the early and late gates can be found in Figure 16. Within the return from of the cloud we find that the correlation coefficient of the early and late gates is approximately -0.8, indicating a high degree of anti-correlation between the gates. Again, there appears to be a special structure associated with the trailing edge of the return from the cloud. Therefore, we shall select four points to examine in more detail; the leading and trailing edges of the cloud (0.55 μs and 3.30 μs), the middle of the cloud (2.00 μs), and from the thermal noise (6.00 μs). A comparison of the Pearson Correlation Coefficient, Spearman Correlation Coefficient, and Kendall's Tau is contained in Table 1. From this table it is clear that all three statistics are in reasonable agreement; hence the plot of the Pearson Correlation Coefficient in Figure 16 is likely to be reliable.

| | Pearson Correlation Coefficient | Spearman Rank-Order Test | Kendall's Tau Test |
|---|---|---|---|
| Point 1 (0.55 μs) | -0.278 | -0.282 | -0.189 |
| Point 2 (3.30 μs) | +0.344 | +0.438 | +0.322 |
| Point 3 (2.00 μs) | -0.862 | -0.859 | -0.676 |
| Point 4 (6.00 μs) | +0.344 | +0.337 | +0.225 |

**Table 1 Comparison of Correlation Coefficient Statistics.**

We can gain a clearer picture of the nature of the two dimensional statistical distribution of the early and late gates by examining the their scatter plots. The scatter plots of each of these samples are shown in Figures 17 through to 20 respectively. From the scatter plot for the leading edge of the chaff return, Figure 17, it can be seen that the distribution has a long tail due to the influence of the chaff cloud; the early gate is in the cloud, whereas the late gate is in the thermal noise. Since the early gate has a long tail, it is clear that the distribution between the early and late gates is not a two dimensional Gaussian distribution. The scatter plot of the return from the trailing edge of the chaff cloud demonstrates that the variance is small, and that a positive correlation between the gates does exist. The best behaved distribution is that

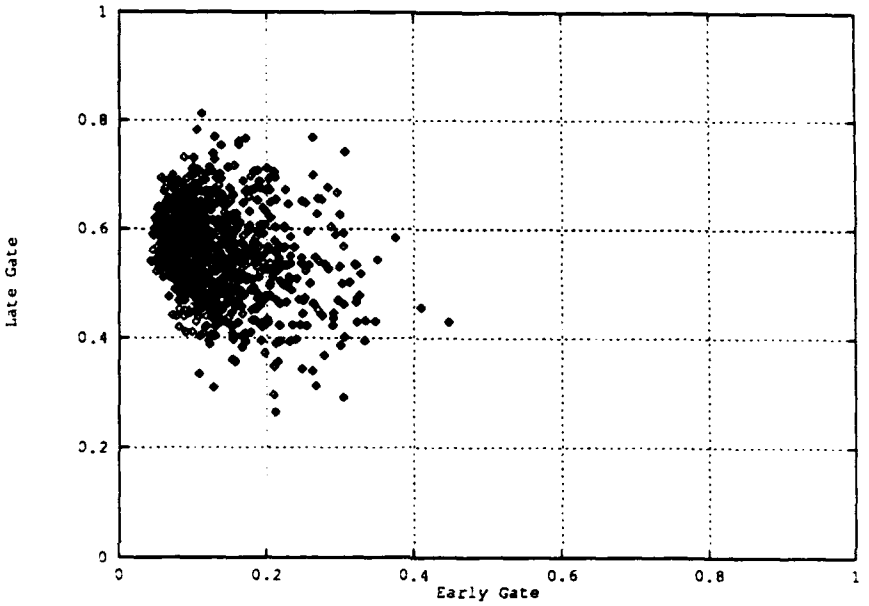


**Figure 17 The scatter plot for the leading edge of the chaff return, for the AGC system, using a 0.1 μs pulse width.**

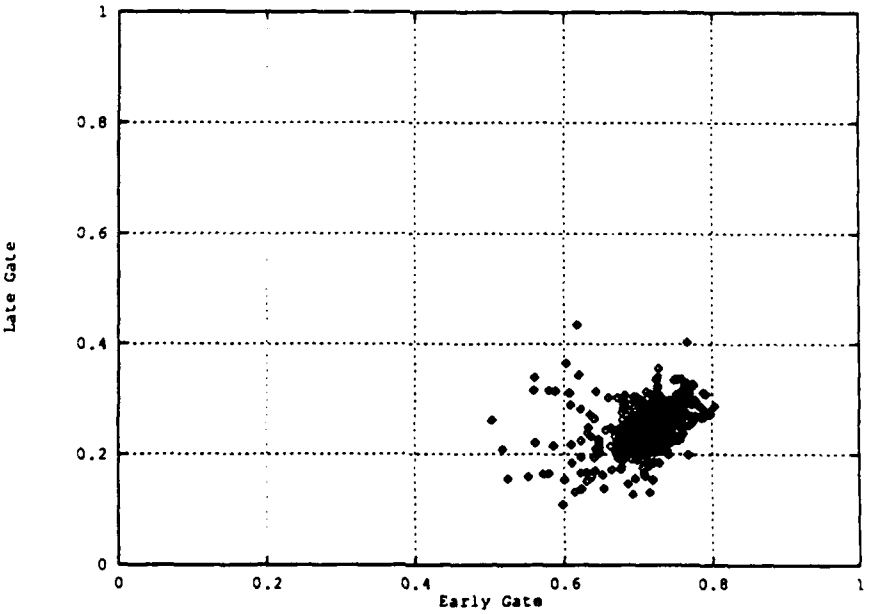


**Figure 18 The scatter plot for the trailing edge of the chaff return, for the AGC system, using a 0.1 μs pulse width.**

from within the chaff cloud, Figure 19. Here, a strong anti-correlation in this distribution is immediately apparent to the eye. This distribution could probably pass for a two dimensional Gaussian distribution. The distribution due to the thermal noise, Figure 20, is also well behaved. Since this return is derived by an averaging process, due to the action of the low-pass filter, we would expect that this distribution would be close to a Gaussian distribution.

In summary, the distributions for the early and late gates for the return due to thermal noise, and the chaff return are easily understood and characterised. Indeed, it is remarkable that the statistical characteristics of

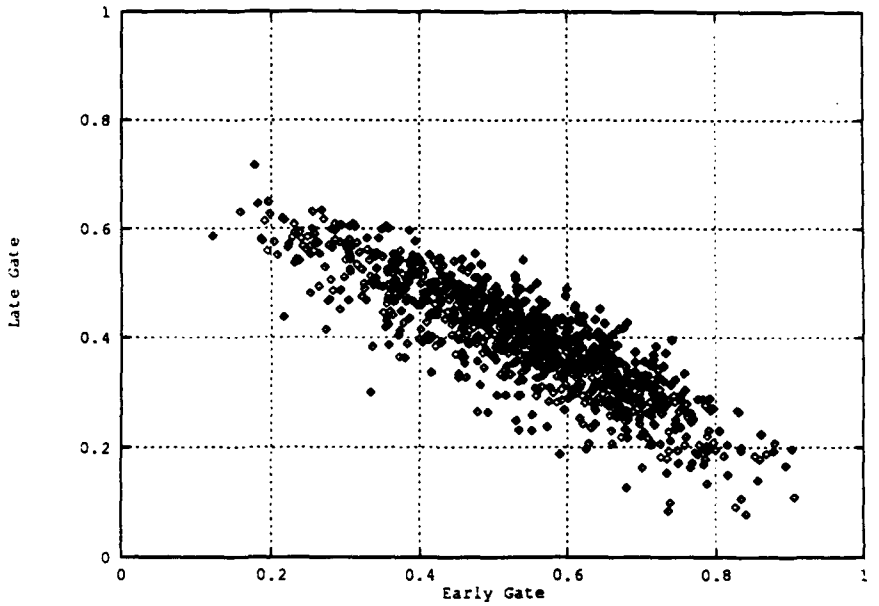


**Figure 19 The scatter plot for a point from within the chaff return, for the AGC system, using a 0.1 μs pulse width.**

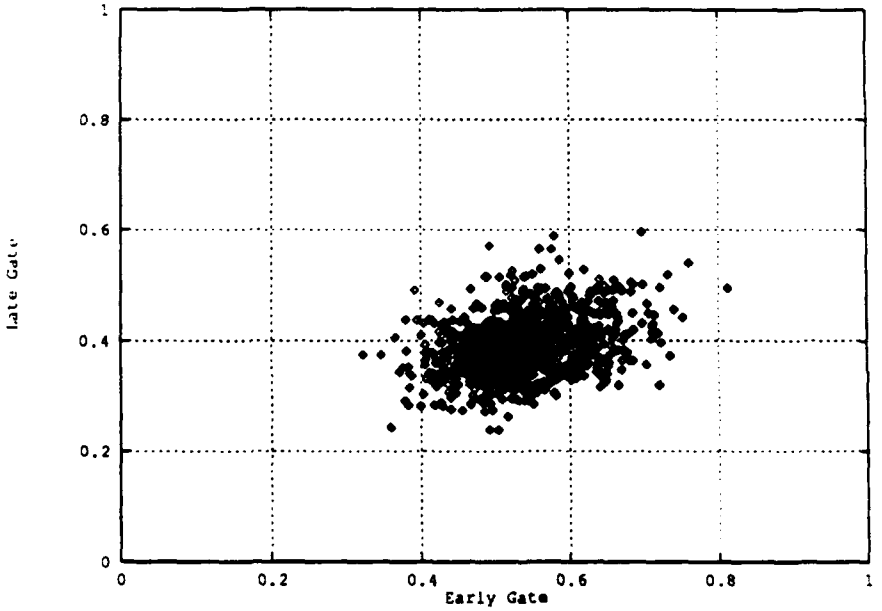


**Figure 20 The scatter plot due to thermal noise alone, for the AGC system, using a 0.1 μs pulse width.**

the chaff cloud as processed by the range discriminant from within the chaff return are so uniform. It is also clear that the leading and trailing edges of the chaff return have their own special structure and that the transition between the signal from within the chaff cloud and the thermal noise is not smooth.

The above analysis is now repeated for the 0.5 μs pulse width. A sample of the range discriminant is given in Figure 21, the average response in Figure 22, the standard deviation of the range discriminant in Figure 23, and the Correlation coefficient in Figure 24. The mean value of the range discriminant has the

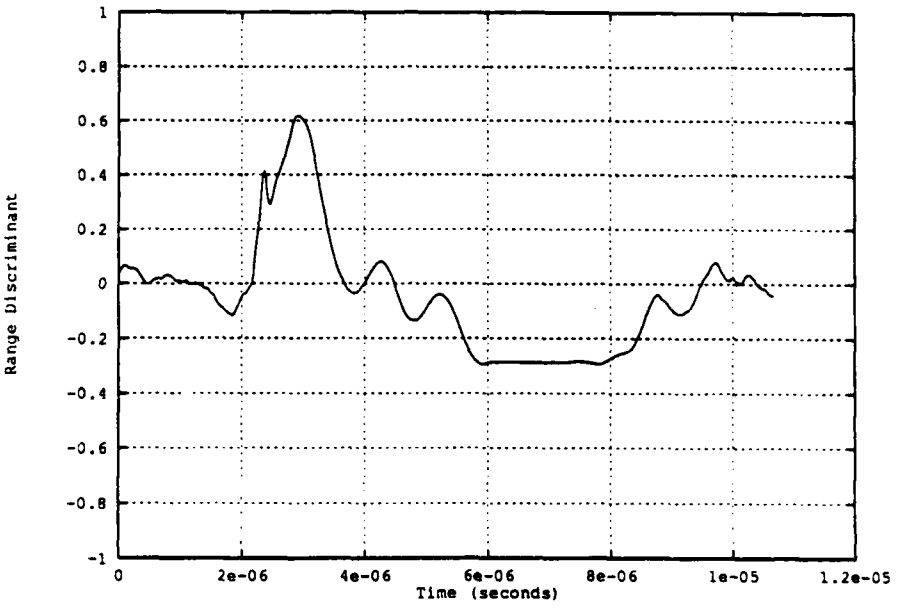


**Figure 21 A random sample of the range discriminant for the AGC system, using a 0.5 μs pulse width.**

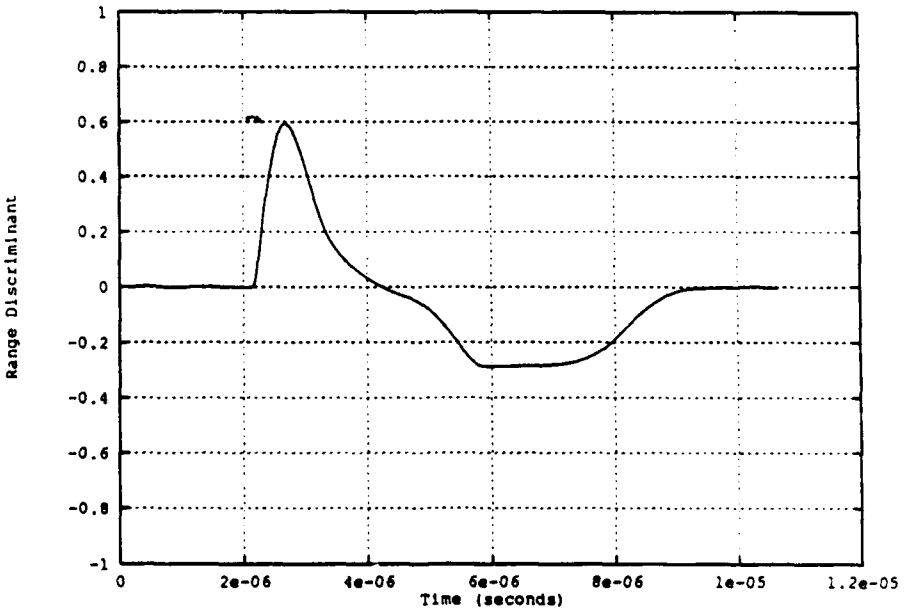


**Figure 22 The average over 1000 samples of the range discriminant for the AGC system, using a 0.5 μs pulse width.**

sort of structure one would expect, except for the long flat negative portion on the trailing edge of the chaff return. This is most likely to be associated with the decay of the output of the matched filter we have used in these calculations. Unlike the previous set of simulations, the structure of the mean value of the range discriminant is visible in the random sample of Figure 21.

On comparing Figure 23 and Figure 24 to their counterparts in the previous simulations (Figures 15 and 16 respectively), we can see that a similar structure occurs. The central portion of the return has the same

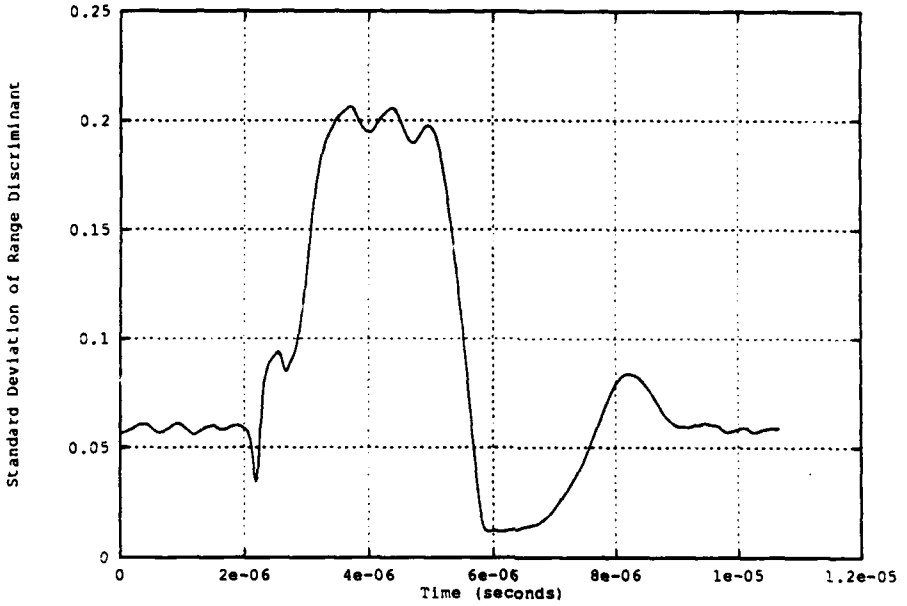


**Figure 23 The standard deviation of the range discriminant for the AGC system, using a 0.5 μs pulse width.**

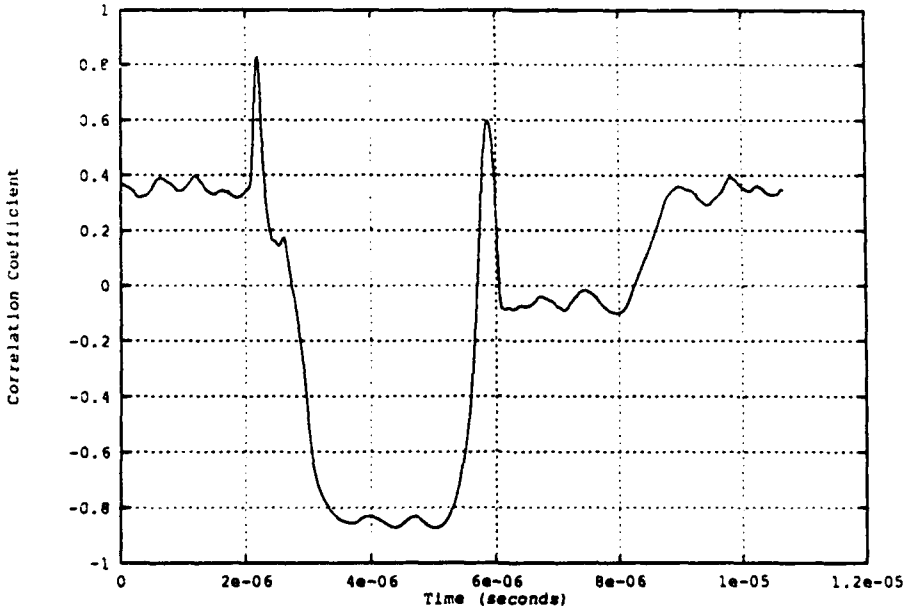


**Figure 24 The correlation coefficient of the early and late gates for the AGC system, using a 0.5 μs pulse width.**

standard deviation and correlation coefficient as that of the previous simulations. However, the observed statistical structure of the leading edge and trailing edges of the cloud, although similar in shape, are more pronounced. This can be explained by the larger pulse length relative to the cloud radius.

To verify the validity of the Pearson Correlation Coefficient used here, a point on the leading edge of the return (2.55 μs), the trailing edge of the cloud (5.87 μs), the middle (4.00 μs), and thermal noise (10.00 μs) were selected, and then examined in more detail. The Pearson Correlation Coefficient, Spearman Rank Correlation Coefficient and the Kendall Tau test were applied, and the agreement between all three tests was similar to that found in the previous set of simulations. The scatter plots for each of these four selected points were similar in appearance to their counterparts in the previous set of simulations, and are therefore omitted.

In summary, the above statistical analysis of the simulation results indicates that the statistical behaviour of the range discriminant operating on the signal return from within the chaff cloud is remarkably uniform. Here, the variance is 0.2, and the correlation coefficient is -0.8, and is easily distinguished from the thermal noise, which due to the filtering action of the low-pass filter has a smaller standard deviation and has a slight positive correlation coefficient. However, the leading edges and trailing edges of the chaff return that are have their own special structure. This structure can be explained by the mixture of the thermal noise signal and the chaff return that occurs at the edges; for example, one gate is within the return from the cloud, while the other is dominated by the thermal noise.

## 4.2 Range Discriminant with a Logarithmic Detector

If the detector is a logarithmic detector, or some reasonable approximation to a logarithmic detector, then the signal power level affects the output by an additive constant. Hence, the slope of a range discriminant based upon the difference between the early and late gates is unaffected by the signal power level, eliminating the need to normalise the difference between the early and late gates. Therefore, apart from an arbitrary multiplicative constant, the range discriminant for a logarithmic detector system can be implemented by Equation 4.2.1.

$$r(t_g) = \int_{-\infty}^{\infty} e(t - t_g)\log|s_o(t)|\,dt - \int_{-\infty}^{\infty} l(t - t_g)\log|s_o(t)|\,dt \qquad 4.2.1$$

Here, $e(t_g)$ and $l(t_g)$ are the early and late gate functions used earlier in the discussion of the discriminant for AGC system. The correlation integrals used here are implemented numerically by a FFT in our simulation program. We normalise these integrals by dividing by twice the pulse width, so that we can sensibly compare the features of the range discriminant with that of the AGC system, and we choose the width of each of these gates to be 0.8 of a pulse width. This allows a direct comparison of the results of this section to that of the AGC system discussed in the previous section.

In principle, we can obtain analytical results for the mean value range discriminant, using the result of Equation 3.2.2. However, due to the effects of thermal noise, which was neglected in this derivation, the results would only be valid where the signal strength from the chaff cloud is large compared to the thermal noise. From the simulations concerning the range discriminant for the AGC system, we see that many of the interesting phenomena are associated with the leading and trailing edges of the return from the chaff cloud, where this assumption is not valid. Furthermore, the analytical problems associated with obtaining the standard deviation and the correlation coefficient prevent useful results being obtained. Hence, to obtain the statistical characteristics of the range discriminant for the logarithmic detector, Monte-Carlo analysis is required.

This range discriminant can be implemented in the radar by passing the signal from each of the early and late gates into a simple low-pass filter. This filter will perform an averaging action over the thermal ensemble, in exactly the same manner as was discussed previously for the AGC system. Since the same sort of physical considerations apply, we use the same filter system driven by the correlation integrals of Equation 4.2.1 to model the range discriminant.

For a 0.1 μs pulsed radar a typical range discriminant is shown in Figure 25; the average response over 1000 samples is shown in Figure 26, and the standard deviation in Figure 27. As with the simulations of the AGC system discussed in the previous section, an individual random sample of the range discriminant does not display the structure apparent in its average response. Also, the standard deviation of the range discriminant operating on the chaff return from within the cloud is uniform, and the trailing edge of the cloud is marked by a dramatic drop in the standard deviation of the range discriminant. Indeed, the overall behaviour of the average value of range discriminant and its standard deviation is very similar to that

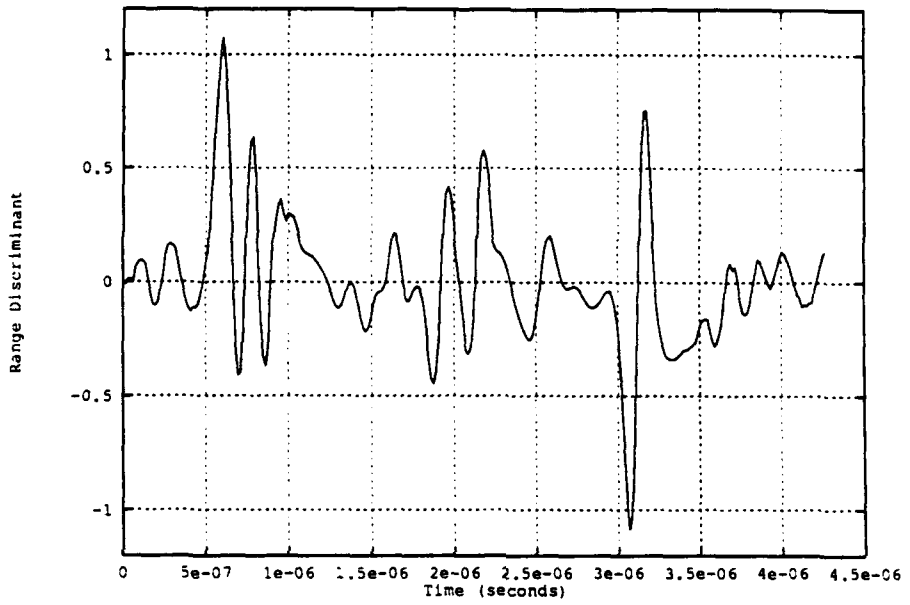


**Figure 25 A random sample of the range discriminant for the Log system, using a 0.1 μs pulse width.**

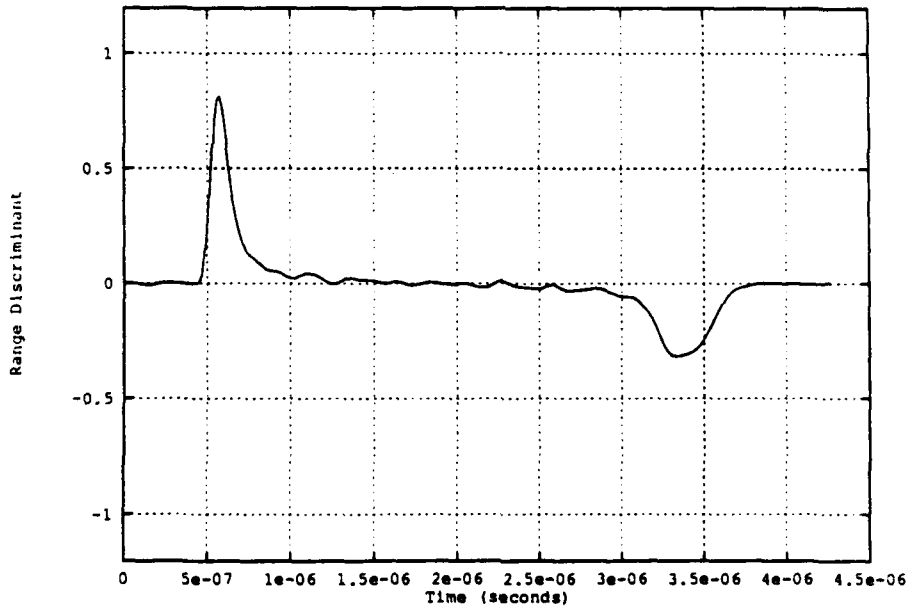


**Figure 26 The average over 1000 samples of the range discriminant for the Log system, using a 0.1 μs pulse width.**

found for the AGC system (compare with Figure 14 and Figure 15).

The Pearson Correlation coefficient of the signal in the early and late gates is given in Figure 28. The thermal noise is characterised by a correlation coefficient of about +0.3, and the return from the middle of the cloud is correlated somewhat more strongly, in as far as we can infer this difference given the sampling fluctuations. The leading edge of the cloud is marked by narrow dip in the correlation of the cloud: one gate within the cloud with the other gate outside the cloud. However, the trailing edge is marked by a broad, strong positive correlation. Overall, the structure of the correlation coefficient here is totally different from

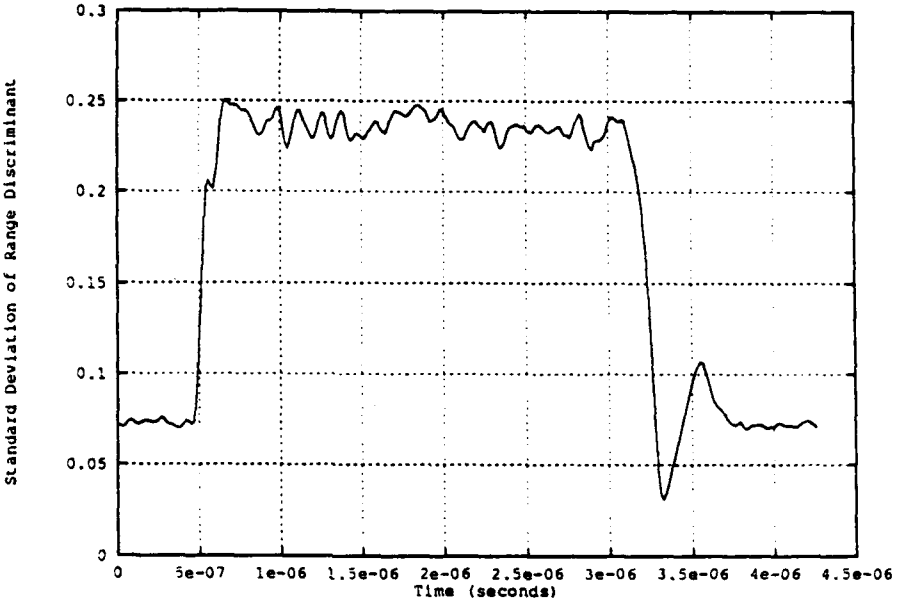


**Figure 27 The standard deviation of the range discriminant for the Log system, using a 0.1 μs pulse width.**

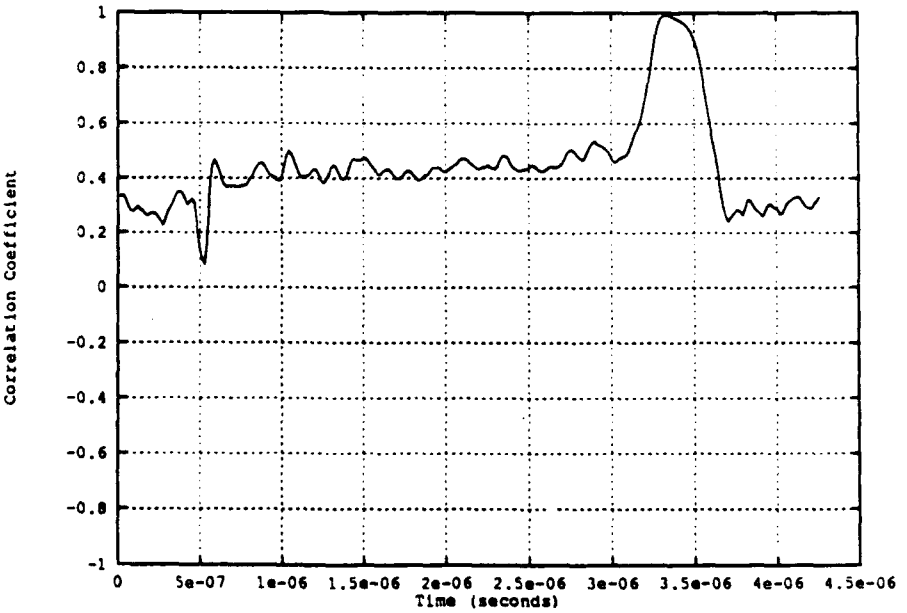


**Figure 28 The correlation coefficient of the early and late gates for the Log system, using a 0.1 μs pulse width.**

that for the AGC system (compare Figure 28 with Figure 16).

As before, we select some points to examine more closely, and perform other statistical tests for correlation coefficient (we choose the same four points as indicated in Section 4.1 for the 0.1 μs simulation); the agreement between teach of these three tests was found to be quite good.

The scatter plot for the leading and trailing edges of the cloud can be found in Figure 29 and Figure 30

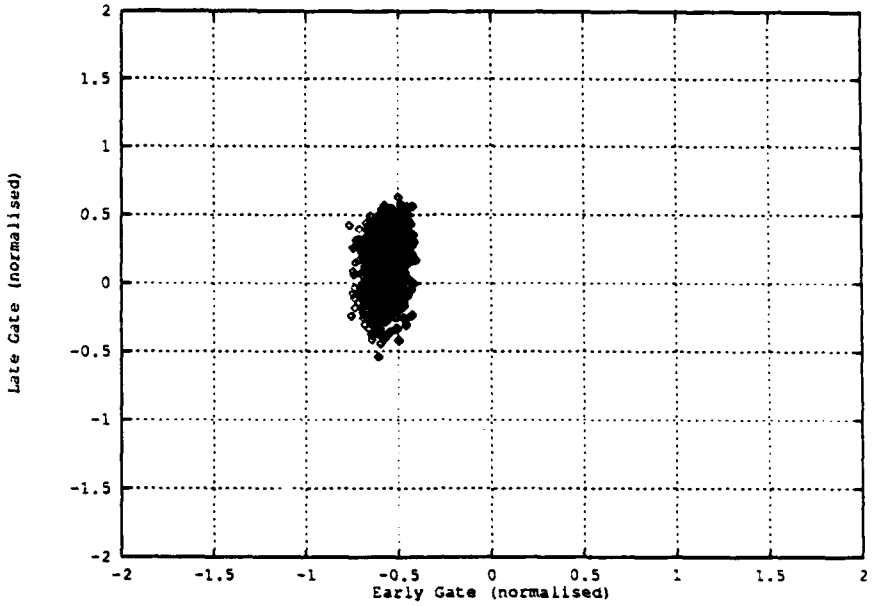


**Figure 29 The scatter plot for the leading edge of the chaff return, for the Log system, using a 0.1 μs pulse width.**

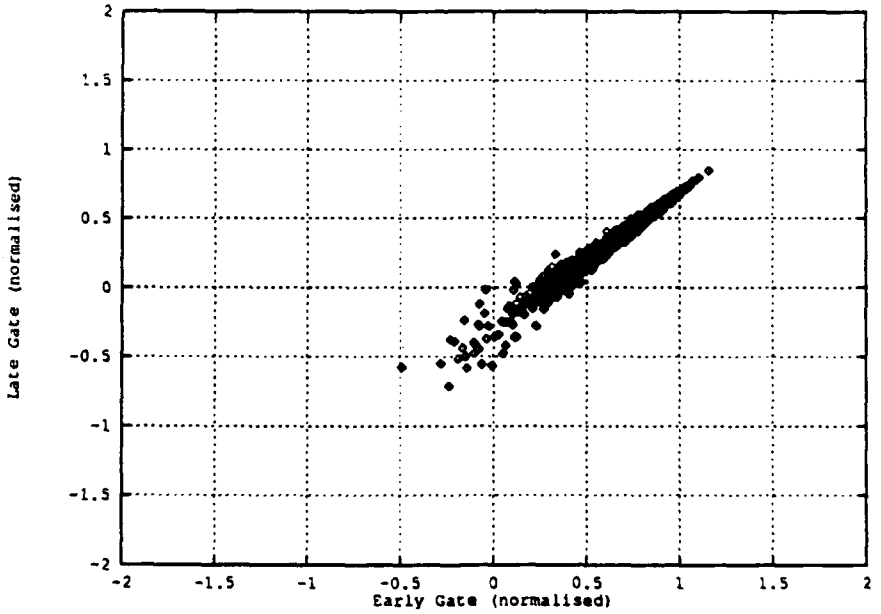


**Figure 30 The scatter plot for the trailing edge of the chaff return, for the Log system, using a 0.1 μs pulse width.**

respectively. The scatter plot for the leading edge of the cloud shows no discernable correlation to the eye, and its appearance indicates it could be modelled by a two dimensional Gaussian distribution. The same cannot be said for the distribution for the trailing edge of the cloud. The large positive correlation in this distribution is immediately apparent to the eye, and the skewed character of the distribution indicates that this distribution is not Gaussian.

The scatter plots for the return from within the cloud, and that due to thermal noise are given in Figures 31

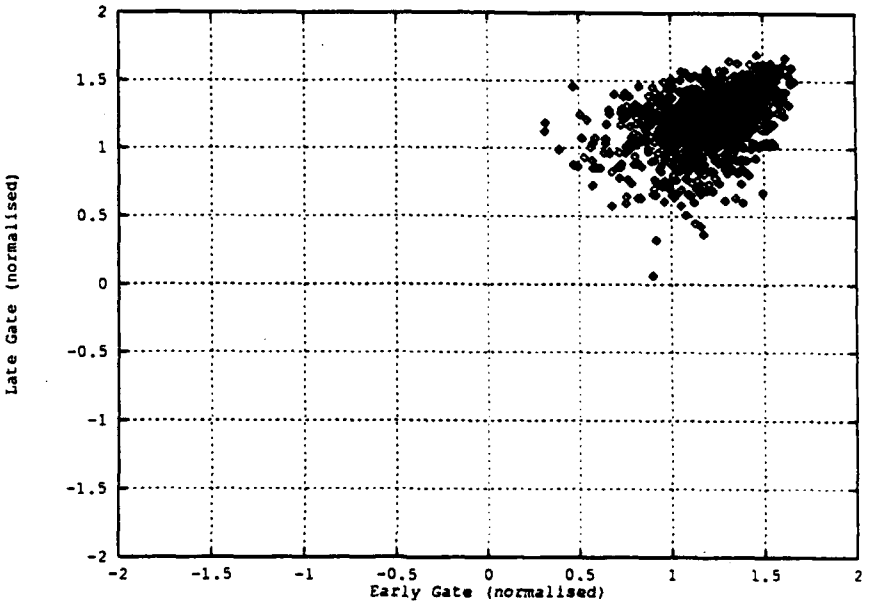


**Figure 31 The scatter plot for the within the chaff return, for the Log system, using a 0.1 μs pulse width.**

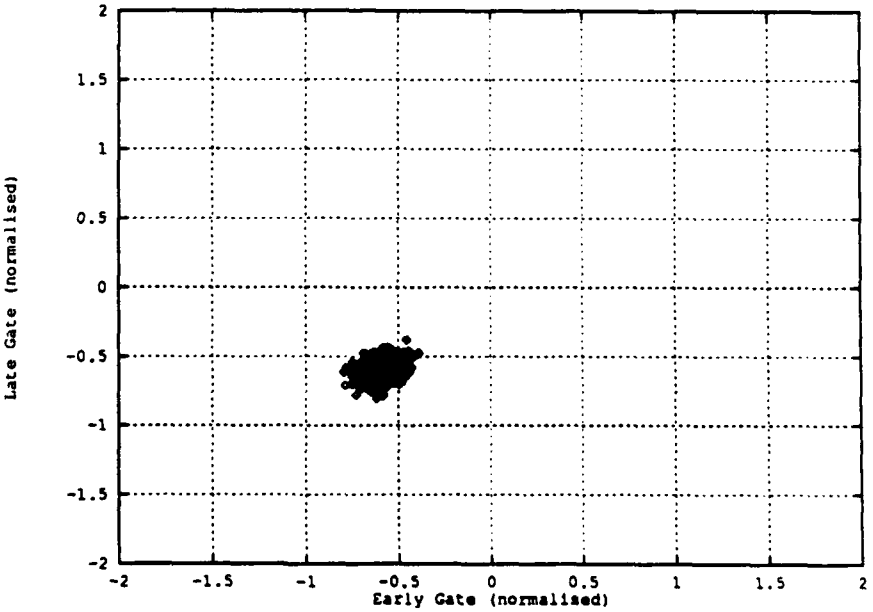


**Figure 32 The scatter plot due to thermal noise alone, for the Log system, using a 0.1 μs pulse width.**

and 32 respectively. In each case a small positive correlation can be detected by eye. The distribution of the return from within the cloud, Figure 31, is skewed, indicating that it is not a Gaussian distribution. The averaging effect over the thermal noise is apparent in the distribution in Figure 32. The variance is smaller, and the shape of this distribution is more nearly elliptical than that of Figure 31.

As we would expect, the nature of the distributions studied here are different from those associated with the AGC system. Nevertheless, the mean and standard deviation of these distributions are similar to their

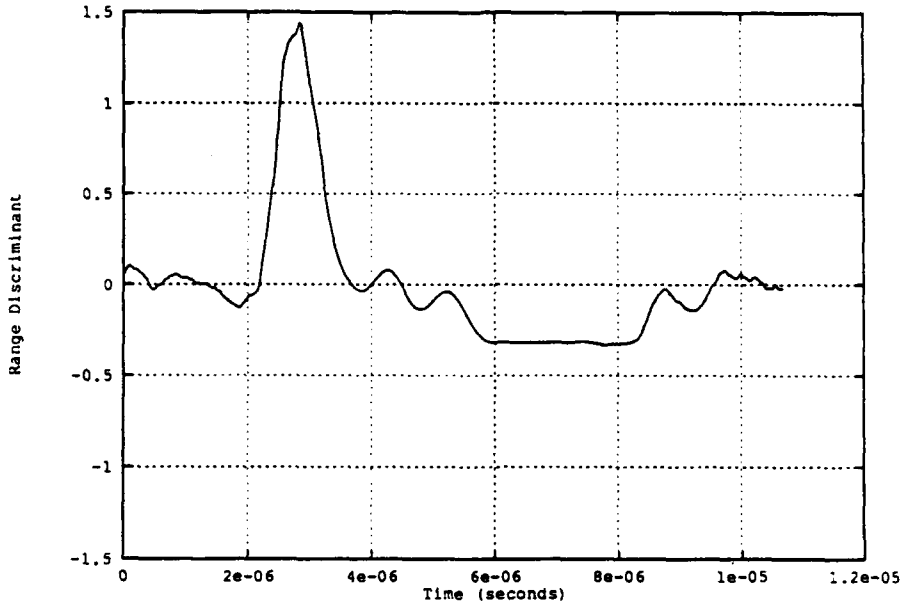


**Figure 33 A random sample of the range discriminant for the Log system, using a 0.5 μs pulse width.**

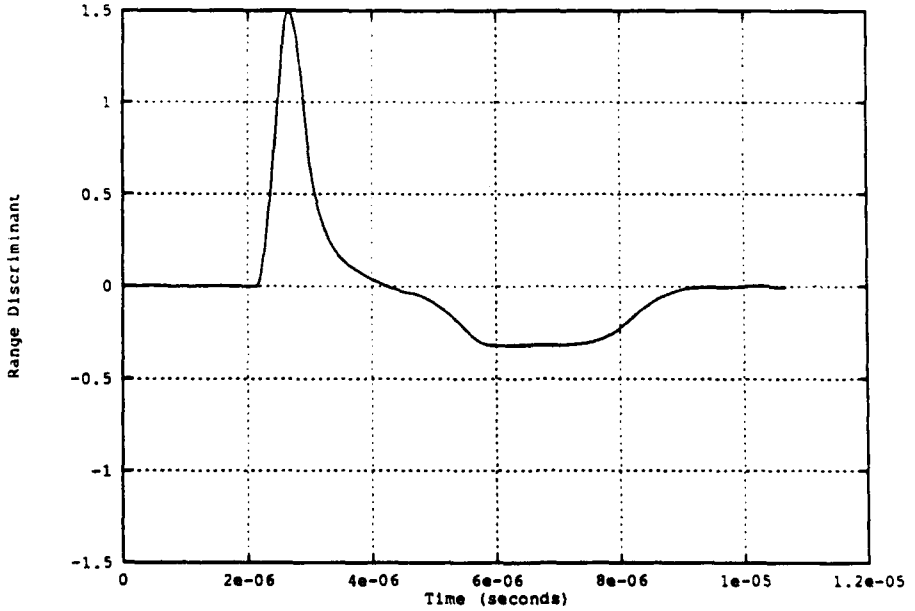


**Figure 34 The average over 1000 samples of the range discriminant for the Log system, using a 0.5 μs pulse width.**

counterparts in the AGC system. The differences lie in the correlation properties between the gates.

We repeat the analysis for the 0.5 μs pulse width radar. A single random sample of the range discriminant is given in Figure 33; the average response over 1000 samples in Figure 34, and the standard deviation in Figure 35.

As far as the mean and standard deviation of the range discriminant are concerned, the results given here

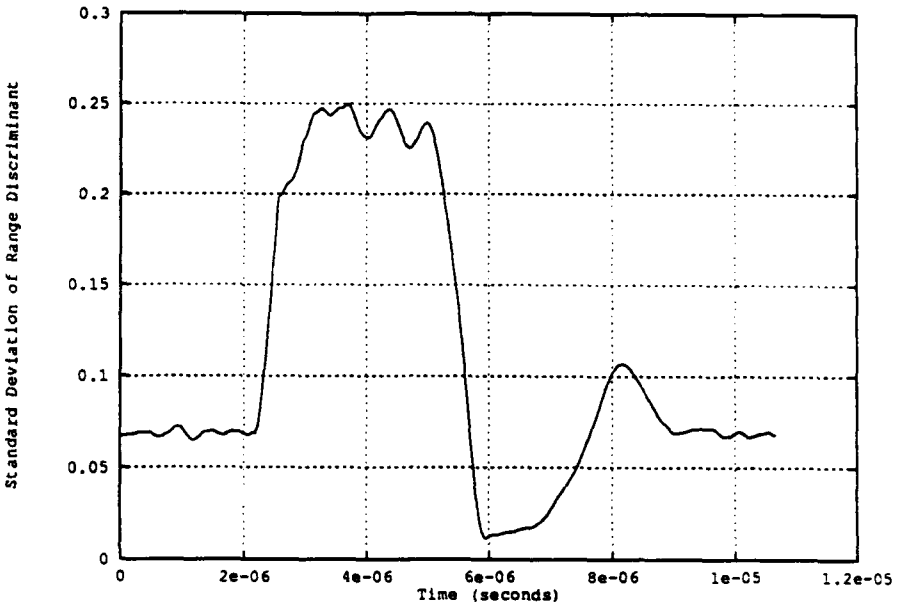


**Figure 35 The standard deviation of the range discriminant for the Log system, using a 0.5 μs pulse width.**

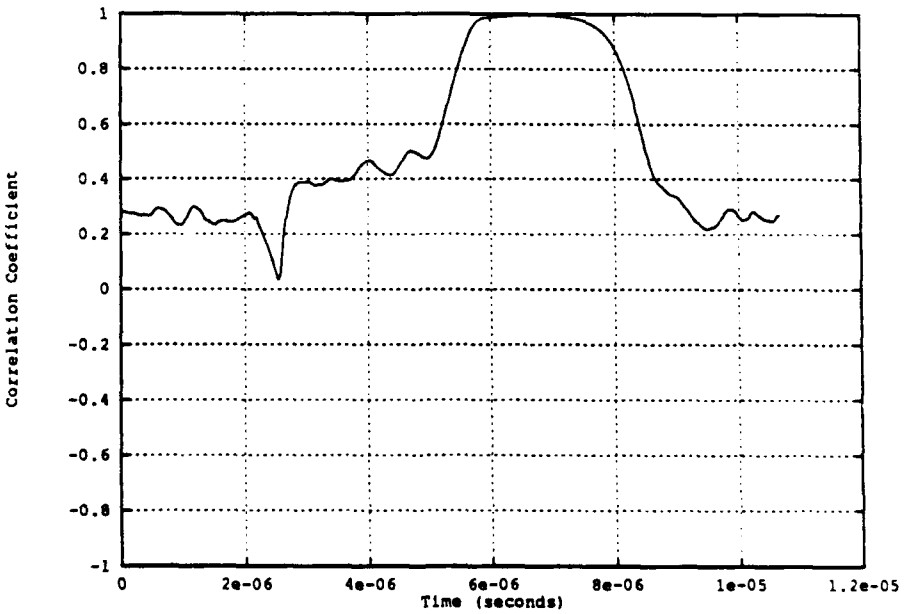


**Figure 36 The correlation coefficient of the early and late gates for the Log system, using a 0.5 μs pulse width.**

are similar to those obtained for the AGC system with 0.5 μs pulse width (compare Figures 33, 34 and 35 to Figures 21, 22 and 23 respectively). The structure seen in the average response (Figure 34) is clearly visible in the random sample (Figure 33). The standard deviation of the range discriminant operating on the return from within the cloud is about 0.2, and the trailing edge of the cloud is marked by a broad dip (Figure 35).

In examining the correlation properties of the early and late gates, Figure 36, we find that there are major differences when compared to the 0.5 μs pulse width AGC system (compare with Figure 24). The leading edge of the cloud is marked by a narrow dip, and the trailing edge displays a large, positive correlation. The scatter plots derived from points on the leading and trailing edge of the cloud are similar to those obtained for the simulation of the 0.1 μs pulse width radar, and are therefore omitted.

In summary, we find that for both of the pulse widths considered in this report, the relationship between the results for the log system range discriminant and that of the AGC system range discriminant are similar. The mean and the standard deviation of the range discriminant is essentially the same, and it is the correlation between the early and late gates that distinguish the two systems.

# 5 DISCUSSION

The radar return from a chaff cloud is inherently statistical, since it is composed of the echoes of a large number of statistically independent scatterers. The advantage of the numerical technique developed in this report is that it generates a random sample of the received field strength from the chaff cloud, after processing by the matched filter. After processing this signal by the detector, we obtain a random sample of the video signal as presented on an A-scope display. Through Monte-Carlo analysis of this signal, as processed by the range discriminant, some insight into the statistical effects associated with a range discriminant operating upon this type of signal has been obtained. This analysis was carried out for a system employing a linear detector with a first order AGC loop, and one using a logarithmic detector. Although we have also obtained the mean power envelope of the received signal, the statistical analysis carried out in this report provides information concerning the statistical characteristics of the range discriminant which cannot be obtained from the mean power envelope of the received signal alone.

The results indicate that as far as the range discriminant is concerned, the statistical characteristics of the return from within the chaff cloud are remarkably uniform, and largely independent of the signal strength. For the AGC system, the average value of the range discriminant is close to zero (see Figures 14 and 26). The standard deviation of the range discriminant was about 0.2 (see Figures 15 and 23). Given that the maximum of the absolute value range discriminant for this system is 0.8, this indicates that the fluctuations of the range discriminant about its average value are quite large (compare Figure 13 to Figure 14, and Figure 22 to Figure 23). The correlation coefficient of the early and late gates was -0.8 (see Figures 15 and 24). This high degree of anti-correlation between the early and late gates demonstrates that the distribution of each of the early and late gates are not independent, and the combination must therefore be considered as a two dimensional distribution. The scatter plot of the early and late gates indicates that the distribution could be approximated by a two dimensional Gaussian distribution (see Figure 19). Thus, the statistical characteristics of the range discriminant for this system, for the part of the signal returned from within the cloud, can be cast into the form a 'black-box' statistical model for the purposes of an engineering analysis of the tracking mechanism. Indeed, the effect of thermal noise upon the range discriminant for this system can also be characterised by a simple statistical model, with the appropriate parameters. However, the leading and trailing edges of the received signal from the chaff cloud exhibit a complex statistical structure which defies such a simple characterisation. Not only do the actual statistical parameters change rapidly with the position of the tracking gate, but the statistical distributions are most definitely non-Gaussian (in particular, see Figure 17). In this case, an explicit simulation of the chaff return, such as that developed in this report, would seem to be the most appropriate way of analysing the effect of the chaff cloud upon the range tracking mechanism.

Similar conclusions can be drawn for the range discriminant operating with the logarithmic detector. The mean value of the range discriminant operating on the signal from within the cloud is close to zero (see Figures 26 and 34).The standard deviation of the range discriminant is about 0.24 (see Figures 26 and 35), indicating that the fluctuations of the range discriminant are quite large (compare Figure25 to Figure 26,

and Figure 33 to Figure 34). In this regime, the correlation coefficient is about +0.4, indicating that the distribution of the early and late gates must also be considered to be a two dimensional distribution (see Figures 28 and 36). However, the scatter plot of the early and late gates (see Figure 31) indicates that the two dimensional distribution of the tracking gates is non-Gaussian. The effect of thermal noise is also simply characterised statistically, and, due to the averaging effect of the first order filter used to implement the integration for the tracking gates, the two dimensional statistical distribution of the early and late gates is approximately Gaussian. As with the AGC system, the leading and trailing edges of the returned signal defy a simple statistical characterisation, and the two dimensional statistical distribution of the early and late gates is most definitely non-Gaussian. Again, an explicit simulation of the returned signal of the type developed in this report is a better method of handling the analysis of the range tracking mechanism.

The ultimate goal in using chaff to protect ships is to either distract, or seduce the range tracking mechanism of the ASM from tracking the ship. If seduction is required, then one obvious requirement is that the return from the chaff cloud be significantly larger than the return from the ship, as processed by the radar seeker in the ASM. A typical ship, like the chaff cloud, is a target whose dimensions are of the same size or larger than the pulse widths considered in this report. Therefore, for an analysis of the seduction process to be valid, the time domain RCS profile of the ship is also required. Although we do not analyse this aspect of the problem in this report, we can make following observations based upon some of the results of this report. The CW RCS of the chaff cloud used in this report, a 200 m radius sphere containing $10^8$ isotropically random half-wave dipoles, was 14740 $m^2$. The effect of the pulse width upon the perceived RCS profile of the chaff cloud can be characterised by a loss relative to the CW RCS. This loss figure varies according to the geometry of the cloud, the pulse width, and the type of detector. A typical loss figure for the 0.1 μs pulse width radar was about 15dB relative to the CW RCS, and for the 0.5 μs pulse width radar 8db. When a pulsed radar with AGC is used, the loss figure was reduced by about 3db. Indeed, typical values for the RCS profile in our simulations for the 0.1 μs pulse width radar was of the order 500 $m^2$, except for the AGC system where a value of 1400 $m^2$ was typical. In view of the fluctuating nature of the radar return from the chaff cloud, these figures should be regarded as representative values only. If we wish to ensure seduction is successful, on the grounds that the RCS profile of the received chaff signal dominates the RCS profile of the ship, then the RCS profile of the ship needs to be significantly less than 500 $m^2$ for the 0.1 μs pulse width radar. It may be possible that such a stringent requirement is not totally necessary, but to prove this would at least require an analysis of the time domain RCS profile of the ship, similar to that developed for the chaff cloud developed in this report.

We now consider the various ways in which calculations of the type performed in this report could be extended. In practice, the cloud will not be spherical, or any other nice geometrical shape. Given that the above results seem to be insensitive to the absolute power levels of the chaff return, it is possible that the statistical characteristics of the range discriminant discussed above will carry over to a more physically realistic cloud shape. The spherical cloud used in this report is not fundamental to the calculations, but a simple shape used to obtain representative results. A more physically realistic shape could be used if desired.

Since we have not included doppler effects, we cannot strictly speaking obtain spectral characteristics of the returned signal with this technique. We can only obtain the return from some randomly chosen configuration of scatterers. In effect, we obtain a random sample from the first order probability distribution in time of the received pulse shape, and the statistical analysis carried out in this report concerns this probability distribution. However, were we to have available a realistic model for the time evolution of the scattering amplitude function of each volume element of the chaff cloud, then the technique used in this report would be suitable for tracing the time evolution of the returned signal from the chaff cloud for a pulsed radar on a pulse by pulse basis. Since we would obtain the matched filtered signal prior to detection, the non-linear processing of this signal can be accurately modelled. The resulting simulation of the time evolution of the range discriminant could be then subjected to a statistical analysis which includes a spectral analysis of the received signal. With the type of non-linear transformations considered in this report, it is clear that any understanding of the spectral characteristics of the received pulse shape after this type of signal processing would be closely interwoven with the first order probability distribution analysed in this report. In short, the type of random sampling developed in this report is a necessary first step towards a more complete understanding of the spectral characteristics of the received pulse shape in this class of radar. It should also be pointed out here that this type of Monte-Carlo statistical analysis need only be performed for a radar with a poor doppler resolution. A coherent system with a

reasonable doppler resolution would avoid non-linear processing of the type analysed in this report so as not to corrupt the spectral content of the received signal. In this case analytical expressions could easily be developed, using the same information concerning the time evolution of the scattering amplitude function of the volume elements within the cloud. This would eliminate the need for an explicit Monte-Carlo simulation proposed here.

Another area where more detailed analysis could be carried out concerns the polarization characteristics of the returned signal. In the single scattering regime, which is covered in this report, we need only determine average back scattering cross section for the given distribution of dipoles (eg: isotropically random, or horizontally random). When a multiple scattering regime is involved, we are forced to consider the bistatic radar cross section. This is best expressed in terms of a Stoke's Vectors and there is some published information available on this subject (Dedrick et al. 1978), (Peebles 1984a, 1984b).

We now consider how best to handle the effects of multiple incoherent scattering. To obtain information concerning the received pulse shape due to scattering from a chaff cloud in this report we have used the concept of the two frequency correlation function as our method of mathematically describing the chaff cloud. Therefore, we must use the multiple scattering theories which at least provide a solution for the two frequency correlation function, using a Stokes's vector representation to account for the inevitable polarisation effects. Once the two frequency correlation has been determined, the sampling theory used in this report can be used to obtain a random sample of the time domain return for a given transmitted pulse shape. Many of the scattering theories of this type for which usable mathematical results can be obtained assume that the particles are large relative to the incident wavelength, which implies that forward scattering is the dominant process (for examples, see Ishimaru 1978, Ishimaru 1975). This simplifying assumption does not apply to chaff clouds. Supposing that the two frequency correlation can be obtained from one such theory, it is unlikely to greatly improve our understanding of the effect of the returned signal upon the range discriminant. The results of the simulations in this report indicate that it is the leading and trailing edges of the returned signal that display unusual behaviour, and it would appear that this behaviour is not sensitive to the details of the shape of the cloud. However, an improved understanding of the two frequency correlation function would greatly improve our understanding of the chaff profile in the sense of providing a more realistic assessment of the received RCS profile of the cloud. It would quantify the spreading out in time of the impulse response of the chaff cloud due to the multiple scattering processes the beam would undergo before emerging from within the cloud.

# 6 CONCLUSIONS

In this report we have developed a technique for the simulation of the time domain return from a chaff cloud suitable for a pulsed radar. A numerical technique was developed which obtains a random sample of the time domain return from a cloud of stationary scatterers. The algorithm consists of obtaining a random sample of the complex Gaussian random series which the two frequency correlation function represents, and using Fourier Transform methods to obtain the received pulse shape given the transmitted pulse shape. This technique is suitable for analysing the effect of the return from a chaff cloud for pulsed radars, since the doppler resolution of this class of radar is sufficiently poor that doppler effects can be ignored. Since the time domain return from the chaff cloud has been sampled, we can compute the effect of non-linear transformations upon this signal directly, with no further approximations.

One application of this technique was to assess the RCS profile perceived by various types of detectors, relative to the RCS of a steady point target. In this way, the RCS profile of the cloud analysed in this report can be compared directly with the available experimental data. Analytical results were compared to simulation results. For the example treated in this report, a 200 m radius sphere containing $10^8$ isotropically random half-wave dipoles, the 0.1 μs pulse width radar experienced losses of about 15dB relative to the CW RCS, and for the 0.5 μs pulse width radar the losses were about 8dB for a radar using a logarithmic detector. When a pulsed radar with AGC is used, these losses were further reduced by about 3db.

A second application of this technique was to examine the statistical behaviour of the range discriminant. The results indicate that the statistical characteristics of the range discriminant operating on the return from within the cloud can be distinguished from that due to thermal noise alone. The transition between the two distinct regimes, the leading and trailing edges of the chaff return, each have their own distinctive statistical characteristics. These characteristics appear to be independent of the pulse widths considered, although

some differences were found between the AGC system and the log detector system. Although we have used a spherical cloud in these calculations, this assumption is not critical, and the results appear to be insensitive to this assumption. Other shapes could easily be used in these calculations if desired.

## ACKNOWLEDGEMENTS

I wish to thank Terry Moon for providing me with an opportunity to make observations of the behaviour of received pulse shapes at the chaff trials discussed in the text, and advice concerning the experimental aspects of chaff measurements. Also, many thanks are due to Gary Watts, who provided highly valued support in the form of programming the algorithms developed in this report into Fortran 77 code. For some discussions concerning the architecture of pulsed radars, I wish to thank Cos Melino. Finally, I wish to thank Bill Dickson for his advice and support in writing this report.

## REFERENCES

J.J.Bowman, T.B.A.Senoir, P.L.E.Uslenghi, 'Electromagnetic and Acoustic Scattering by Simple Shapes', Hemisphere Publishing Corporation, 1969; (see Chapter 12)

K.D.Dedrick, A.R.Hessing, G.L.Johnson, 'Bistatic Radar Scattering by Randomly Orientated Wires', IEEE Trans. Antennas and Propagation, Vol.AP-26, No.3, May 1978, p420

R.Deutsch, 'NonLinear Transformations of Random Processes', Prentice-Hall, 1962

A.Ishimaru, 'Correlation functions of a wave in a random distribution of stationary and moving scatterers', Radio Science, Vol.10, No.1, January 1975, p45

A.Ishimaru, 'Wave Propagation and Scattering in Random Media', Academic Press, 1978

C.L.Mack, B.Reiffen, 'RF Characteristics of Thin Dipoles', Proc. IEEE, Vol.52, May 1964, p533

R.L.Mitchell, 'Radar Signal Simulation', Artech House, 1976

J.E.Ohlson, 'Exact Dynamics of Automatic Gain Control', IEEE Trans. Communications, January 1974, p72

P.Z.Peebles Jr., 'Bistatic Radar Cross Sections of Chaff', IEEE Trans. Aerospace and Electronic Systems, Vol.AES-20, No.2, March 1984, p128

P.Z.Peebles Jr.,'Bistatic Radar Cross Section of Horizontally Oriented Chaff', IEEE Trans. Aerospace and Electronic Systems, Vol.AES-20, No.6, November 1984, p798

W.H.Press, B.P.Flannery, S.A.Teukolsky, W.T.Vetterling, 'Numerical Recipes (Fortran Version)', Cambridge University Press, 1986

S.O.Rice, 'Mathematical Analysis of Random Noise', Bell System Technical Journal, 1944, Vol.23 p282, Vol. 24, p46

D.C.Schleher, 'Introduction to Electronic Warfare', Artech House, 1986

H.L.Van-Trees, 'Detection, Estimation, and Modulation Theory, Vol.III', John Wiley and Sons, 1971

J.H.Van-Vleck, F.Bloch, M.Hamermesh, 'Theory of Radar Reflections from Wires or thin Metallic Strips', Journal Applied Physics, Vol.18, March 1947, p274

# APPENDIX I THE SCATTERING CROSS SECTION OF RANDOMLY ORIENTATED DIPOLES ACCORDING TO THE CHU RESONANCE FORMULAE

In this Appendix we compute the average total scattering cross section for a randomly orientated half wave and full wave dipole, using the Chu resonance formula for the bistatic radar cross section. We consider first isotropically random orientation for the dipoles, then horizontally aligned random orientated dipoles. In all cases we only consider a linearly polarised incident wave, thus avoiding the need to invoke the Stokes's parameters.

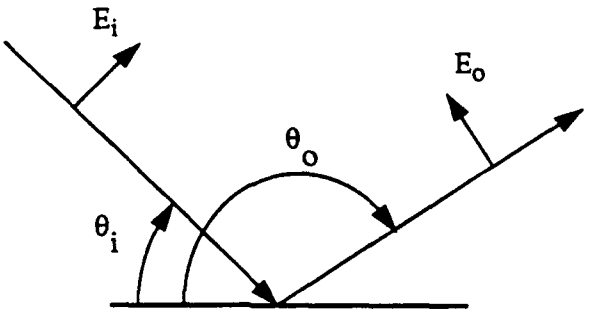


**Figure I.1 Incident and scattered angle geometry.**

The Chu resonance formulae for the bistatic radar cross section is given in Equations I.1 and I.2 for the half wave dipole and the full wave dipole respectively (see for example, Mack, Reiffen 1964). Here, $\theta_i$ and $\theta_o$ are the angles defined by the propagation of the incident and scattered waves respectively to the axis of the dipole (see Figure 37). The component of the field vector normal to the axis of the dipole cannot induce a current along the dipole axis. Therefore these formulae refer to the radar cross section of the component of the field along the dipole axis.

$$\sigma(\hat{o}, \hat{i}) = \sigma(\theta_o, \theta_i) = C_h \lambda^2 \left( \frac{\cos\frac{\pi}{2}\cos\theta_o}{\sin\theta_o} \right)^2 \left( \frac{\cos\frac{\pi}{2}\cos\theta_i}{\sin\theta_i} \right)^2 \quad \text{I.1}$$

$$\sigma(\hat{o}, \hat{i}) = \sigma(\theta_o, \theta_i) = C_f \lambda^2 \left( \frac{\sin\pi\cos\theta_o}{\sin^2\theta_o} \right)^2 \left( \frac{\sin(\pi\cos(\theta_i))}{\sin^2\theta_i} \right)^2 \quad \text{I.2}$$

The values of $C_h$ and $C_f$ can be derived from a suitable normalisation of the gain patterns, and are given by:

$$C_h = \frac{4}{\pi} \left( \int_0^{\pi} \left( \frac{\cos\frac{\pi}{2}\cos\theta}{\sin\theta} \right)^2 \sin\theta d\theta \right)^{-2} \quad \text{I.3}$$

$$C_f = \frac{4}{\pi} \left( \int_0^{\pi} \left( \frac{\sin\pi\cos\theta}{\sin^2\theta} \right)^2 \sin\theta d\theta \right)^{-2} \quad \text{I.4}$$

These quantities can be evaluated in terms of the Si and Ci integrals (see for example Wolff 1988), or evaluated numerically using the mathematical package of your choice.

The Chu Resonance formula does not include the effect of losses in the scatterer. Hence, the total scattering cross section will be approximated here by the scattering cross section:

$$\sigma_t(\hat{i}) \approx \sigma_s(\hat{i}) = \frac{1}{4\pi}\int_{4\pi} \sigma_b(\hat{o}, \hat{i})d\Omega_o \qquad \text{I.5}$$

In this case, the total scattering cross section for a given incident angle in the thin wire geometry is:

$$\sigma_t(\hat{i}) = \sigma_t(\theta_o) = \frac{1}{2}\int_0^{\pi} \sin\theta_o \sigma_b(\theta_o, \theta_i)d\theta_o \qquad \text{I.6}$$

These formulae need to be related to the dipole geometry as shown in Figure 38. To obtain the appropriate geometrical transformations of the angles involved we follow the treatment of Dedrick et al. (1978). The orientation of the dipole relative to the incident plane wave is described by the angles $(\theta,\phi)$. The vector triad $(\hat{n}, \hat{l}, \hat{r})$ forms a right handed system of unit vectors; $\hat{n}$ is the unit vector in the direction of propagation, and the electric field is in the plane defined by $\hat{l}$ and $\hat{r}$. Since we shall only be considering linearly polarised waves, we shall assume that the incident electric field is along the $\hat{l}$-axis only.

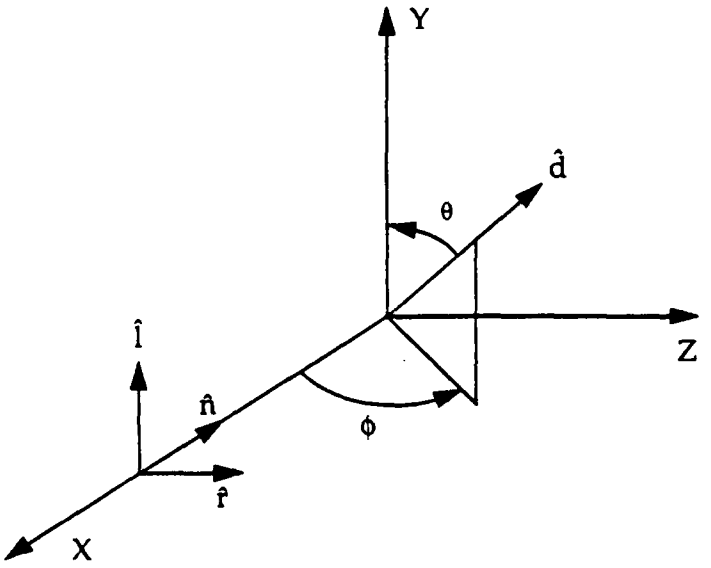


**Figure I.2 Co-ordinate for dipole orientation used in average RCS calculation.**

A key feature of the geometry of the thin wire geometry is that only the component of the electric field in the plane formed by the dipole and the direction of the plane wave propagation will cause an induced current. Hence, we need to compute the component of the electric field along the dipole, given the orientation of the dipole relative to the incident wave vector. Straightforward computation shows that the component of $\hat{E}_l$ along the dipole axis, $\hat{E}_p$, is given by:

$$\hat{E}_p = \begin{bmatrix} 0 \\ \dfrac{\cos\theta\sin\theta\sin\phi}{\cos^2\theta + \sin^2\theta\sin^2\phi} \\ \dfrac{\cos^2\theta}{\cos^2\theta + \sin^2\theta\sin^2\phi} \end{bmatrix} \qquad \text{I.7}$$

$$\frac{1}{2}\left|\hat{\mathbf{E}}_p\right|^2 = \frac{1}{2}\left|\hat{\mathbf{E}}_i\right|^2 \frac{\cos^2(\theta)}{\cos^2(\theta) + \sin^2(\theta)\sin^2(\phi)} \qquad \text{I.8}$$

Hence, providing we can relate the thin wire geometry angle $\theta_i$ to the dipole orientation specified by the angles $(\theta,\phi)$, the scattering cross section is

$$\sigma_t(\theta,\phi) = \sigma_t(\theta_i)\frac{\cos^2\theta}{\cos^2\theta + \sin^2\theta\sin^2\phi} \qquad \text{I.9}$$

The average value of the scattering cross section, given a uniform distribution over $(\theta,\phi)$, is therefore

$$\langle\sigma_t\rangle = \frac{1}{4\pi}\int_{4\pi}\left(\sigma_t(\theta_i)\frac{\cos^2\theta}{\cos^2\theta + \sin^2\theta\sin^2\phi}\right)\sin\theta d\theta d\phi \qquad \text{I.10}$$

To simplify this integral, we transform the variables $(\theta,\phi)$ to $(\theta_i,\phi_i)$ via A1.11, following Dedrick et al. (1978).

$$\begin{aligned}\cos\theta_i &= \sin\theta\cos\phi \\ \cos\phi_i &= \frac{\cos\theta}{\sin\theta_i} = \frac{\cos\theta}{\sqrt{1-\sin^2\theta\cos^2\phi}}\end{aligned} \qquad \text{I.11}$$

The range of $(\theta_i,\phi_i)$ is that of $(\theta,\phi)$. Some straightforward but tedious algebra shows that the Jacobian of this transformation is

$$\left|\frac{\partial(\theta_i,\phi_i)}{\partial(\theta,\phi)}\right|^{-1} = \left|\frac{\sin\theta_i}{\sin\theta}\right| \qquad \text{I.12}$$

Hence, the integral for the average scattering cross section in this case becomes:

$$\begin{aligned}\langle\sigma_t\rangle &= \frac{1}{4\pi}\int_{4\pi}\sigma_t(\theta_i)\cos^2\phi_i\sin\theta_i d\theta_i d\phi_i \\ &= \frac{1}{4}\int_0^{\pi}\sigma_t(\theta_i)\sin\theta_i d\theta_i\end{aligned} \qquad \text{I.13}$$

Thus, the average of the scattering cross section over all orientations can be written as the product of two identical one dimensional integrals. Indeed, if Equations I.1 and I.2 respectively are substituted into Equation I.13, and simplified according to Equations I.3 and I.4, the final result is

$$\langle\sigma_t\rangle = \frac{1}{2\pi}\lambda^2 \approx \lambda^2(0.159154943\ldots) \qquad \text{I.14}$$

This result holds for both half-wave and full wave dipoles, with isotropically random orientation. The standard expressions for the average back scattering cross section and the co-polarised back scattering cross section are easily derived from the above analysis, and the results are those quoted in the body of this report.

When the dipoles assume a random orientation in the plane of the incident radiation, the algebra is considerably simpler (ie: $\phi$=0, $\theta$ is random). In this case the average scattering cross section for an incident field polarised in the plane of the dipoles is given by:

$$\langle\sigma_t\rangle = \frac{1}{\pi}\int_0^{\pi}\sigma_s(\theta_i)d\theta_i \qquad \text{I.15}$$

The result for the half dipole is:

$$\langle\sigma_t\rangle = \lambda^2\frac{2}{\pi^2}\left(\left(\int_0^{\pi}\left(\frac{\cos\frac{\pi}{2}\cos\theta}{\sin\theta}\right)^2 d\theta\right)\Big/\left(\int_0^{\pi}\left(\frac{\cos\frac{\pi}{2}\cos\theta}{\sin\theta}\right)^2\sin\theta d\theta\right)\right) \qquad \text{I.16}$$

$$= \lambda^2(0.2335158427\ldots)$$

For the full wave dipole, the result is:

$$\langle\sigma_t\rangle = \lambda^2\frac{2}{\pi^2}\left(\left(\int_0^{\pi}\left(\frac{\sin\pi\cos\theta}{\sin^2\theta}\right)^2 d\theta\right)\Big/\left(\int_0^{\pi}\left(\frac{\sin\pi\cos\theta}{\sin^2\theta}\right)^2\sin\theta d\theta\right)\right) \qquad \text{I.17}$$

$$= \lambda^2(0.3861911457\ldots)$$

The integrals can be expressed in the form of Si and Ci integrals, or evaluated with the mathematical package of your choice.

## REFERENCES

K.D.Dedrick, A.R.Hessing, G.L.Johnson 'Bistatic Radar Scattering by Randomly Orientated Wires', IEEE Trans. Antennas and Propagation, Vol.AP-26, No.3, May 1978, p420

C.L.Mack, B.Reiffen 'RF Characteristics of Thin Dipoles', Proc. IEEE, Vol.52, May 1964, p533

E.A.Wolff 'Antenna Analysis', Artech House, 1988

# APPENDIX II THE SCATTERING FUNCTION FOR A DISTANT SPHERICAL CLOUD OF UNIFORMLY DISTRIBUTED SCATTERERS

In this Appendix we calculate the scattering function for a distant, spherical cloud of uniformly distributed scatterers; that is, a cloud which is wholly contained within the 3dB beam width of the radar. The basic formulae for $\Sigma(R)$ is:

$$\Sigma(R) = P_0 \int_A \left( \frac{G_t(\hat{i})}{G_t(\hat{i}_0)} \right)^2 \left( \frac{R_0}{R} \right)^4 \rho \langle \sigma_b \rangle \exp(-2\langle \gamma \rangle) dA \qquad \text{II.1}$$

$$P_0 = P_t \frac{\lambda^2}{(4\pi)^3} \frac{G_t(\hat{i}_0)^2}{R_0^2} \qquad \text{II.2}$$

Here, $P_0$ is the power that would be received from a point target with unity radar cross section. For a distant cloud of uniformly distributed scatterers, we approximate Equation II.1 by

$$\Sigma(R) \approx P_0 \int_A \rho \langle \sigma_b \rangle \exp(-2\langle \gamma \rangle) dA \qquad \text{II.3}$$

For a spherical cloud of radius $R_c$, whose centre is located at range $R_0$ from the radar we obtain:

$$\Sigma(R_0 + z) = P_0 \int_0^{\sqrt{R_c^2 - z^2}} (2\pi r dr) \rho \langle \sigma_b \rangle \exp(-2\rho \langle \sigma_t \rangle (\sqrt{R_c^2 - r^2} - |z|)) \qquad \text{II.4}$$

$$= P_0 \left( 2\pi \frac{\langle \sigma_b \rangle}{2\langle \sigma_t \rangle} \right) \exp(-2\rho \langle \sigma_t \rangle z) \left( \exp(-2\rho \langle \sigma_t \rangle |z|) \left( |z| + \frac{1}{2\rho \langle \sigma_t \rangle} \right) \right.$$
$$\left. - \exp(-2\rho \langle \sigma_t \rangle R_c) \left( R_c + \frac{1}{2\rho \langle \sigma_t \rangle} \right) \right)$$

As discussed in the main text, the critical parameter is the ratio of the mean free path of scattering to the radius of the cloud, $\rho \langle \sigma_t \rangle R_c$. If this value is small relative to unity, then Equation II.4 becomes:

$$\Sigma(R_0 + z) \approx P_0 \rho \langle \sigma_b \rangle (R_c^2 - z^2) \qquad \text{II.5}$$

The Continuous Wave (CW) RCS of the cloud, $\Sigma_0$, given by the integral of $\Sigma(R)$ over the range of R. Thus,

$$\Sigma_0 = P_0 \int_{-R_c}^{R_c} \Sigma(R) dR = \left( \frac{\langle \sigma_b \rangle}{2\langle \sigma_t \rangle} \right) \left( \pi R_c^2 + \frac{\pi R_c}{2\rho \langle \sigma_t \rangle \exp(4\rho \langle \sigma_t \rangle R_c)} \right.$$
$$\left. - \frac{\pi}{8(\rho \langle \sigma_t \rangle)^2} + \frac{\pi R_c}{8(\rho \langle \sigma_t \rangle)^2 \exp(4\rho \langle \sigma_t \rangle R_c)} \right) \qquad \text{II.6}$$

In the limit of small values of $\rho \langle \sigma_t \rangle R_c$, where shielding effects are negligible, it is easily shown that Equation II.6 becomes:

$$\Sigma_0 \approx \frac{4}{3} \pi R_c^3 \rho \langle \sigma_b \rangle \qquad \text{II.7}$$

THIS IS INTENTIONALLY BLANK

| DISTRIBUTION | Copy No. |
|---|---|
| DEPARTMENT OF DEFENCE | |
| *Defence Science and Technology Organisation* | |
| Chief Defence Scientist | ) 1 Shared Copy |
| DSTO Central Office Executive | ) for circulation |
| Counsellor Defence Science, London | Control Sheet Only |
| Counsellor Defence Science, Washington | Control Sheet Only |
| *Electronics Research Laboratory* | |
| Director, Electronic Research Laboratory | 2 |
| Chief, Electronic Warfare Division | 3 |
| Research Leader, Electronic Countermeasures | 4 |
| Head, Electronic Countermeasures Group | 5 |
| *Surveillance Research Laboratory* | |
| Director, Surveillance Research Laboratory | 6 |
| Chief, Microwave Warfare Division | 7 |
| Head, Microwave Radar Systems | 8 |
| *Navy Office* | |
| Navy Scientific Adviser | 9 |
| Director of Naval Warfare | 10 |
| Director of Naval Communications, Command and Control, Computers and Intelligence | 11 |
| Director of Electronic Warfare and Intelligence | 12 |
| *Army Office* | |
| Scientific Adviser - Army | 13 |
| *Air Office* | |
| Air Force Scientific Adviser | 14 |
| Commanding Officer, Electronic Warfare Operations Support Unit | 15 |
| *SA to DIO* | 16 |
| *SA to DC* | 17 |
| *Libraries and Information Services* | |
| AGPS | 18 |
| Librarian, Technical Reports Centre, Defence Central Library, Campbell Park | 19 |
| Manager, Document Exchange Centre Defence Information Services | 20 |
| Defence Research Information Centre, United Kingdom | 21-22 |
| National Technical Information Service, United States | 23-24 |
| Director Scientific Services, Canada | 25 |
| Ministry of Defence, New Zealand | 26 |
| National Library of Australia | 27 |

## DOCUMENT CONTROL DATA SHEET

Security classification of this page : UNCLASSIFIED

| 1 DOCUMENT NUMBERS | | 2 SECURITY CLASSIFICATION | |
|---|---|---|---|
| AR Number: | AR-006-974 | a. Complete Document: | Unclassified |
| Series Number: | ERL-0634-RR | b. Title in Isolation | Unclassified |
| Other Numbers: | | c. Summary in Isolation | Unclassified |
| | | 3 DOWNGRADING / DELIMITING INSTRUCTIONS | |
| | | N/A | |

**4 TITLE**

A TIME DOMAIN SIMULATION OF THE PULSED RADAR RETURN FROM A CHAFF CLOUD

| 5 PERSONAL AUTHOR (S) | 6 DOCUMENT DATE |
|---|---|
| Thomas A. Winchester | May 1992 |
| | 7 7.1 TOTAL NUMBER OF PAGES: 52 |
| | 7.2 NUMBER OF REFERENCES: 15 |

| 8 8.1 CORPORATE AUTHOR (S) | 9 REFERENCE NUMBERS | |
|---|---|---|
| Electronics Research Laboratory | a. Task: | DST 89/114 |
| | b. Sponsoring Agency: | DSTO |
| 8.2 DOCUMENT SERIES and NUMBER | 10 COST CODE | |
| Research Report 0634 | | |

| 11 IMPRINT (Publishing organisation) | 12 COMPUTER PROGRAM (S) (Title (s) and language (s)) |
|---|---|
| Defence Science and Technology Organisation Salisbury | |

**13 RELEASE LIMITATIONS** (of the document)

Approved for Public Release.

Security classification of this page : UNCLASSIFIED

Security classification of this page : UNCLASSIFIED

**14 ANNOUNCEMENT LIMITATIONS** (of the information on these pages)

No limitation.

| **15 DESCRIPTORS** | | **16 COSATI CODES** |
|---|---|---|
| a. EJC Thesaurus Terms | Chaff<br>Radar signals<br>Time domain<br>Pulse radar<br>Monte carlo method<br>Ship defense systems | 1709<br>150601<br>170403 |
| b. Non - Thesaurus Terms | | |

**17 SUMMARY OR ABSTRACT**
(if this is security classified, the announcement of this report will be similarly classified)

A numerical technique for the time domain simulation of the radar return from a chaff cloud is developed. This technique is suitable for pulsed radars. A Monte-Carlo analysis of the effect of this return upon the range discriminant of typical pulsed radar systems is then carried out.